The Effect of the Seasonal Variation of Stratification on the Circulation of the Northern Gulf of California

E. PALACIOS-HERNÁNDEZ

Departamento de Oceanografía Física, CICESE, Ensenada, Baja California, Mexico

E. BEIER

Departamento de Oceanografía Física, CICESE, Ensenada, Baja California, Mexico, and College of Oceanic and Atmospheric Sciences, Oregon State University, Corvallis, Oregon

M. F. LAVÍN AND P. RIPA

Departamento de Oceanografía Física, CICESE, Ensenada, Baja California, Mexico

(Manuscript received 14 February 2000, in final form 22 May 2001)

ABSTRACT

Direct current measurements reveal that the circulation of the northern Gulf of California in the annual timescale consists of a cyclonic basinwide gyre (~0.35 m s^{-1}) that lasts from June to September (4 months), and an anticyclonic gyre (~0.35 m s^{-1}) lasting from November to April (6 months). The transitions between regimes take about three weeks each. The hypothesis that the difference in duration of the two circulation regimes is due to the seasonal variation of stratification of the water column is explored by simulations with a nonlinear two-layer numerical model of circulation and thermodynamics that includes vertical mixing, parameterized as an entrainment velocity. The model results agree remarkably well with the observations, considering its simplified vertical structure. In addition, the model predicts a net circulation consisting of an anticyclonic gyre of ~0.05 m s^{-1}, with a corresponding average concavity of the interface, and a two-layer exchange through the main channels of the archipelago.

1. Introduction

It has been observed that the main feature of the circulation in the northern Gulf of California (henceforth NGC; Fig. 1) is an almost basinwide seasonal gyre, cyclonic in summer and anticyclonic in winter: Lavín et al. (1997) first observed this feature with satellite-tracked drifters; Soto-Mardones et al. (1999) used 14 years of infrared satellite images to show that the feature is persistent; and Bray (1988) and Carrillo et al. (2001) used hydrographic data banks and geostrophic calculations to describe the seasonal evolution. Both gyres have speeds of the order of 0.35 m s^{-1}, but while in summer it is strongly baroclinic, in winter it is a mixture of baroclinic and barotropic (Lavín et al. 1997). Within the limitations imposed by data from different years and by geostrophic calculations, Carrillo et al. (2001) proposed that the cyclonic gyre lasts about 4 months, the anticyclonic gyre about 6 months, and that the transitions between regimes last about 1 month. Bray (1988) applied EOF analysis to a subset of the data used by Carrillo et al. (2001) to describe this reversal and the difference in speed and duration of the geostrophic flow through a cross-section of the NGC. No other measurements exist to confirm this description of the seasonal cycle.

Numerical modelers have offered an explanation for that circulation pattern. Beier (1997, hereafter B97) and Beier and Ripa (1999) obtain the seasonally reversing circulation of the NGC with a two-layer linear numerical model driven by forcing mechanisms that have annual periodicity: in decreasing order of importance, (i) an internal Kelvin-line perturbation of the pycnocline at the mouth of the gulf as proposed by Ripa (1990, 1997), (ii) the monsoonal winds that blow from the northwest in winter and from the southeast in summer, and (iii) the seasonal surface heat flux. Forcing mechanisms (i) and (ii) turn out to be dominant, to produce perturbations similar in shape (internal Kelvin-like), and also to be in phase; the passing of the waveform through the NGC causes the pycnocline to become convex (domeshaped) in summer and concave in winter, and thus the seasonal circulation pattern. The barotropic component seems to be caused by the interaction of the annual internal wave-

Corresponding author address: Dr. M. F. Lavín, CICESE-Oceanography, P.O. Box 434844, San Diego, CA 92143-4844.
E-mail: mlavin@cisese.mx

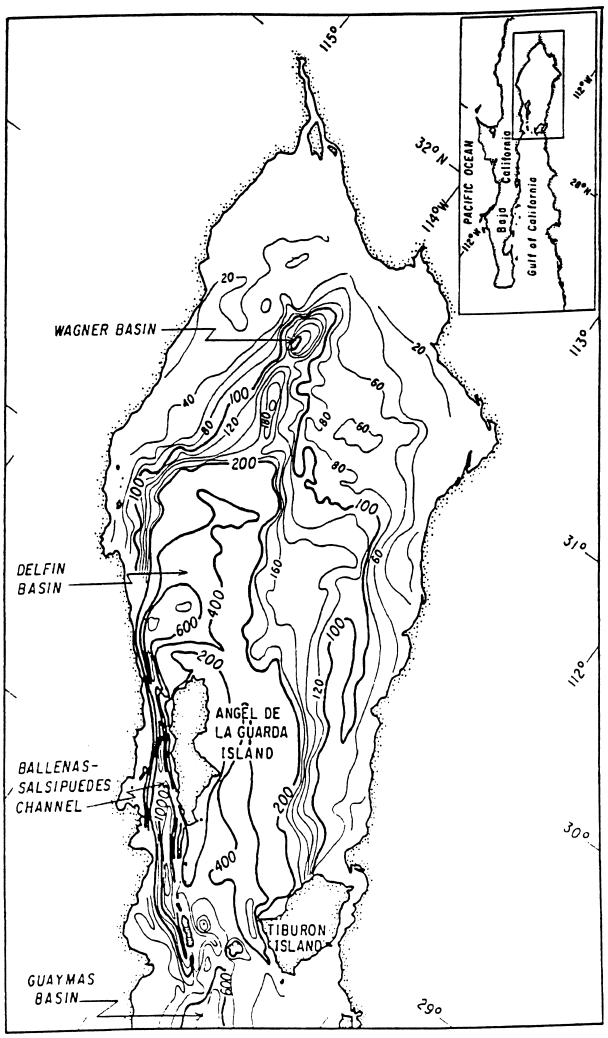

FIG. 1. Bathymetry and basins of the northern Gulf of California (depth in meters).

forms with the bathymetry and the coastline (Beier and Ripa 1999).

There is, however, an aspect of the oceanography of the NGC that, although recognized by the above authors to be of great importance for the circulation, is missing in the numerical models: the seasonal change of stratification of the water column. In winter, the surface mixed layer can reach 90m while in summer it is only a few meters deep (Martínez-Sepúlveda 1994), and stratification as measured by the potential energy anomaly Φ (defined below) presents a strong seasonal signal with a minimum in winter (Argote et al. 1985, 1995). The numerical model of B97 does not include vertical mixing, and stratification changes only with the local variation of the surface temperature produced by the annual surface heat flux; in addition, being linear and forced by annual sinusoids, it produces anticyclonic and cyclonic periods that last 4 months each, with 2 month-long transition periods.

This work provides the first directly observed description of the seasonal evolution of the circulation of the NGC: it is found that the duration of the two main regimes are indeed different. The hypothesis that the seasonal variation of stratification causes the time asymmetry of the circulation pattern is then explored numerically, by nonlinearizing the numerical model of B97 and by adding to it the process of vertical mixing, parameterized as entrainment enhanced by winter upwelling. The simulations are found to agree remarkably well with the observations.

2. Observations

Data

The data used here were collected as part of an observational program carried out between December 1994 and March 1996, which consisted of a series of CTD surveys and the continuous maintenance of a number of current meter moorings, plus the deployment of a few WOCE/ARGOS drifters. Details of the surveys and the current meter data are reported by Palacios-Hernández et al. (1997). The hydrographic data were collected with a factory-calibrated SeaBird CTD, model SBE-911 plus. In this work we use data from four surveys, three made from the R/V *Francisco de Ulloa* and one from the R/V *El Puma* (see Fig. 2). The CTD data were processed as in García-Córdova et al. (1996).

Geostrophic currents were calculated (10 m referred to 100 m) as in Carrillo-Bibriezca (1996), from the vertical integration of the thermal wind equation, using the hydrographic field. In order to produce regularly spaced grids, to decrease subjectivity in the interpretation of the results, and to obtain a better presentation of the data objective mapping was used as described by Roemmich (1983) and used by Bray (1988) for the Gulf of California. The estimated value at the grid nodes is determined by the surrounding data, weighted according to the distance between them. It is assumed that the fields can be decomposed into two scales: a large scale in which properties vary slowly and is insensible to details and a small scale that is only just resolved by the hydrography (Roemmich 1983). Initially, the maximum value corresponded to the scale at which there existed a minimally significant correlation between observations ($\sim$80 km), and the minimum value of the scale was selected as that characterizing exponential decay of $\sim$20 km. Both values were fitted by trial and error. In the horizontal, objective mapping of the dynamic height was used to produce data on a 21 $\times$ 21 grid with geographic limits from 29.5° to 31°N and from 112.5° to 114.5°W. The grid size is 0.075° in latitude and 0.1° in longitude. In the vertical cross sections, objective mapping was applied to the density anomaly on a 31 $\times$ 31 element grid. A more detailed description of the error and correlation analysis in the objective mapping can be seen in Carrillo et al. (2001). Geostrophic

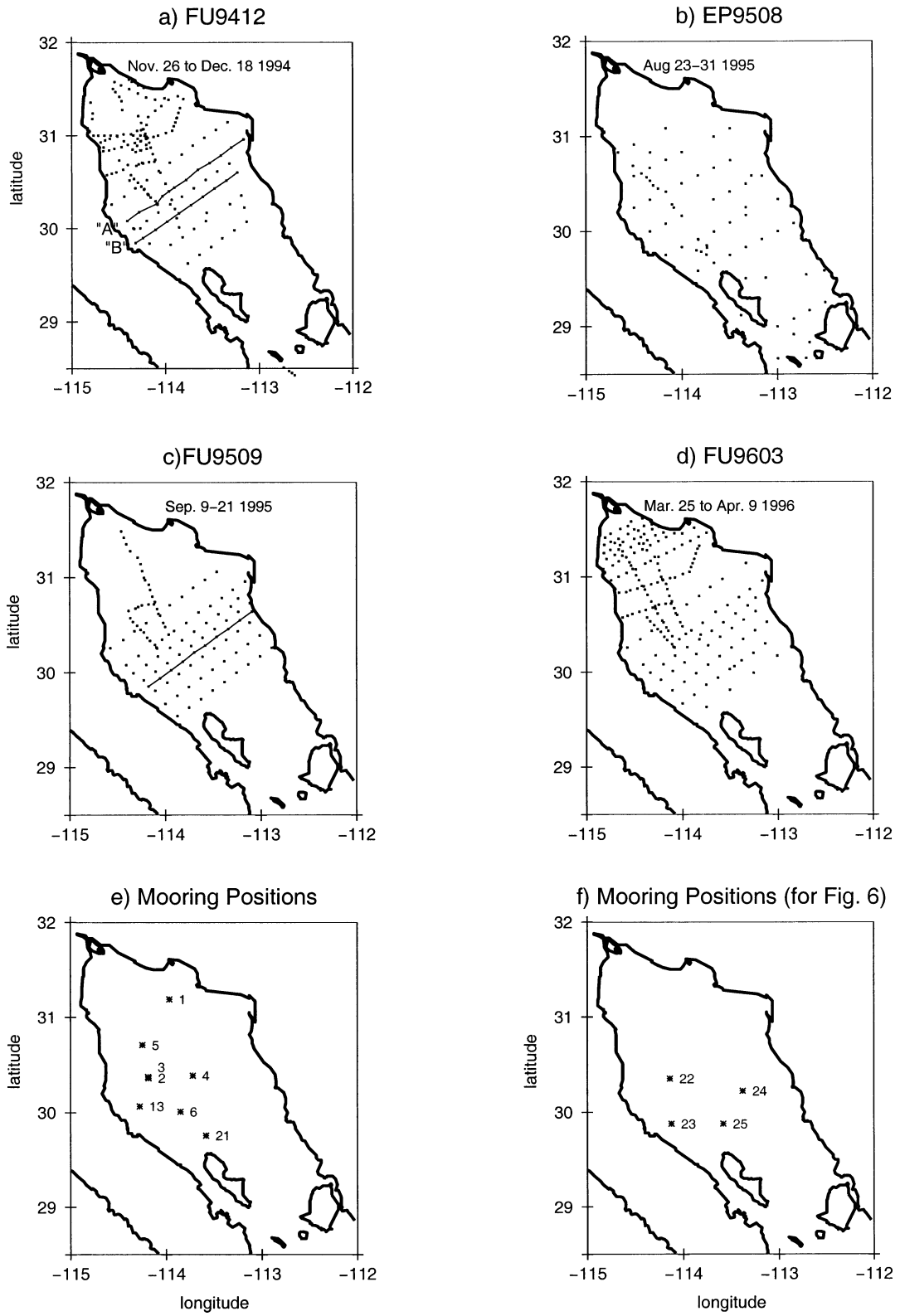

FIG. 2. Positions of CTD stations and current meter moorings: (a) CTD stations made during survey FU9412 campaign (transversal transects A and B indicated by lines); (b) EP9508 campaign; (c) FU9509 campaign (transversal transect are indicated); (d) FU9603 campaign. (e) Current meter mooring positions. (f) Position of moorings of data depicted in Fig. 6.

TABLE 1. Current meter data.

Mooring	Position	Current meter	Depth/bottom (m)	Dates
01	31°11.32′N,	Endeco	19/52	29 Nov–
	113°57.87′W	General Oceanics	29/52	4 Dec 1994
02	30°21.75′N,	General Oceanics	21/150	30 Nov–
	114°10.98′W	General Oceanics	60/150	11 Dec 1994
		General Oceanics	120/150	
03	30°22.50′N,	General Oceanics	21/150	15–29 Dec 1994
	114°11.36′W	General Oceanics	60/150	
		General Oceanics	120/150	
04	30°23.33′N,	General Oceanics	25/150	29 Nov–
	113°43.32′W	General Oceanics	120/150	29 Dec 1994
05	30°42.52′N,	Endeco	28/95	9–29 Dec 1994
	114°14.92′W	General Oceanics	85/95	
06	30°00.62′N,	General Oceanics	20/397	2–29 Dec 1994
	113°51.03′W	General Oceanics	57/397	
		General Oceanics	197/397	
13	30°24.30′N,	General Oceanics	38/200	16 Sep–
	114°16.53′W	General Oceanics	120/200	13 Oct 1995
21	29°45.44′N,	General Oceanics	20/300	20 Sep 1995–
	113°16.79′W			4 Feb 1996
22	30°22.24′N,	General Oceanics	50/205	19 Sep 1995–
	114°11.77′W			26 Feb 1996
23	29°52.57′N,	General Oceanics	50/340	12 Oct 1995–
	114°07.38′W	Aanderaa	100/340	26 Feb 1996
24	30°13.44′N,	General Oceanics	20/145	12 Oct 1995–
	113°22.84′W	General Oceanics	50/145	26 Feb 1996
		General Oceanics	85/145	
25	29°52.69′N,	General Oceanics	20/300	13 Oct 195–
	113°34.95′W			26 Feb 1996

velocity was calculated using the bottom as reference level, and the cross-sectional average [$O(1\ \text{cm s}^{-1})$] was subtracted to attain volume balance.

Stratification is measured by means of the potential energy anomaly

$$\Phi = \frac{1}{h}\int_{-h}^{0} gz(\overline{\rho} - \rho(z))\, dz,$$

where h is depth, g is the gravitational acceleration, $\rho(z)$ is the density profile, and

$$\overline{\rho} = \frac{1}{h}\int_{-h}^{0} \rho(z)\, dz$$

(Simpson 1981); Φ is the amount of energy needed to vertically mix the water column to a depth h, which in this case was chosen as 200 m or to the bottom (whichever was shallower).

The current meter data were obtained at different depths and positions, as indicated in Table 1; the position of the moorings whose data are used here are shown in Figs. 2e,f [for full details, see Palacios-Hernández et al. (1997)]. The current meter data were filtered with Godin's filter in order to remove diurnal and semidiurnal tides (Godin 1988) and then sampled once or twice a day.

Five WOCE/ARGOS drifters were deployed on 11 September 1995. Four were recovered and redeployed in March 1996. The last day of useful drifter data is 6 July 1996. These are the same drifters reported by Lavín et al. (1997), but in this paper the complete series is shown and analyzed in more detail. The drifters were programmed to sample continuously for the first 50 days after deployment and then change to a 1 day on/2 days off cycle. Linear interpolation was used to obtain positions every six hours, from which velocities were computed.

3. Observational results

Carrillo et al. (2001) describe the seasonal evolution of the geostrophic circulation of the NGC as two main regimes with vorticity of opposite sign, and transition periods between them: the *anticyclonic period* is loosely associated with winter conditions, while the *cyclonic period* occurs in summer. This nomenclature is followed here, but the duration of each period is more precisely defined for the present observations.

a. Cyclonic regime

The cyclonic (summer) regime has been described as the most clearly persistent (Lavín et al. 1997; Soto-Mardones et al. 1999; Carrillo et al. 2001) and the one with the strongest geostrophic currents. The conditions in the two surveys carried out in August and September 1995 (Fig. 3) are similar, with slightly slower currents in September. The cyclonic gyre dominated the circulation with mean velocities of $\sim$0.40 m s^{-1} (Figs. 3a and 3b), and stratification was very strong (Figs. 3c and

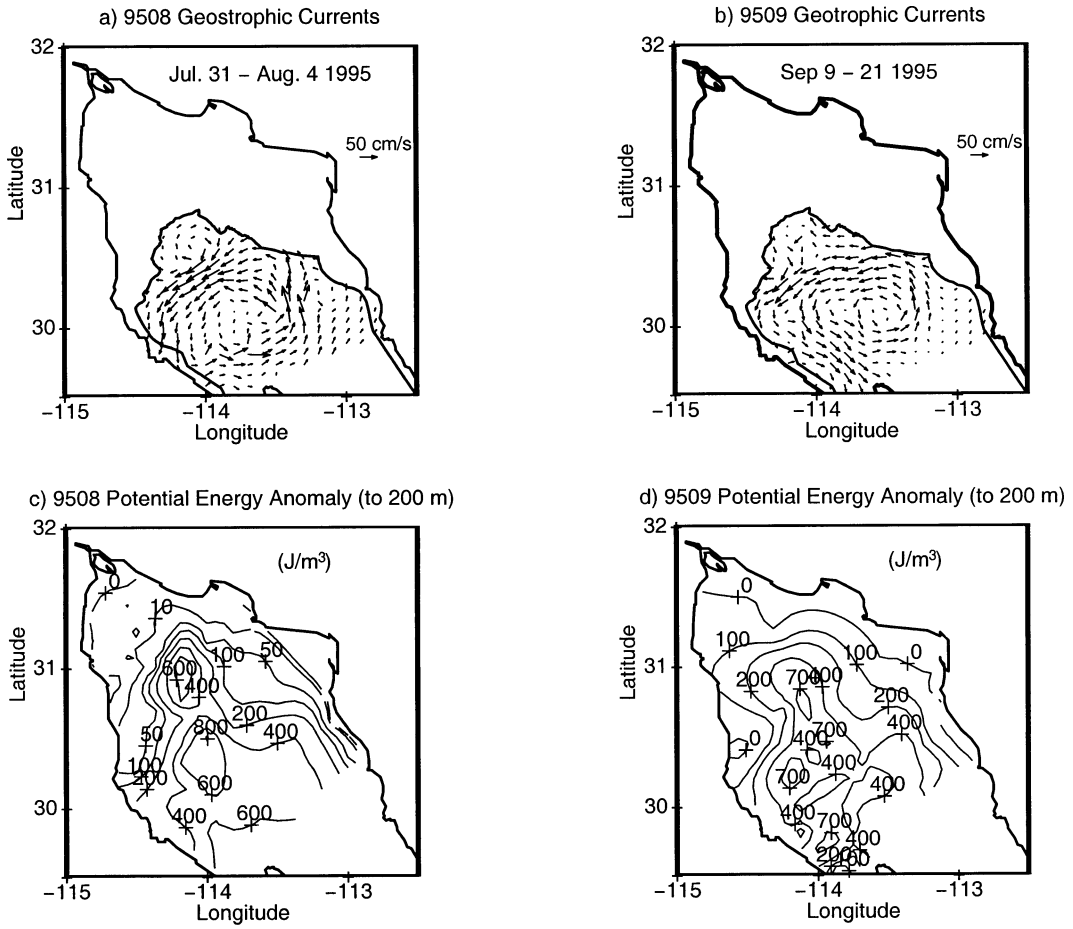

FIG. 3. Geostrophic currents at 10 m referred to 100 m, for (a) EP9508 campaign and (b) FU9509 campaign (the 100-m isobath is indicated). Potential energy anomaly Φ (to 200 m) for campaigns (c) EP9508 and (d) FU9509. Contours for Φ are 0, 10, 100, 200, 400, 600, 700, and 800 J m^{-3}.

3d) with values of Φ reaching from 600 to 700 J m^{-3} in the deeper zones.

The five drifters were launched for the first time during the second cruise, and Fig. 4a shows their velocities ($\sim$0.50 m s^{-1}) during the 18 days after their release. There is a remarkable overall agreement between the surface drifter data and the geostrophic calculations, which has already been pointed out by Lavín et al. (1997). The low-passed time series of the current meters located between 20 and 50 m below the surface for the period 19–27 September 1995 [only mooring 21 began on 29 September; the other moorings began on 21 and 22 September (Fig. 4b)] also captured the cyclonic circulation, showing speeds of the order of 0.30 m s^{-1}. The vertical shear between the current meters (50 m) and the drifters (5–15 m) is due to the baroclinicity of the gyre, as shown in Fig. 5, which is a cross section of density and geostrophic velocity. Figure 5b indicates that the gyre was about 80 m thick and highly baroclinic; the current meter series at 100 m (Fig. 4b) is in agreement with this with almost no speed, which is also shown in the cross section (Fig. 5b). The vertical shear observed by current-meters is 0.0011 s^{-1}, while the geostrophic one is 0.0015 s^{-1}.

b. Autumn transition (from cyclonic to anticyclonic)

Of particular interest in this study is the time of onset and duration of the transition periods. Since no direct observations have so far been available, the best estimates are those of Carrillo et al. (2001), who suggest that the transition takes place in October and lasts about one month. This transition was recorded by current meters and drifters in October 1995.

Figure 6 shows the low-passed current meter data from 19 September 1995 to 22 February 1996. The transition takes place between 28 September and 18 October. This is very hard to recognize in the time series, but it is well revealed by an EOF analysis (Fig. 7). The first mode (58% of the variance explained) has a spatial distribution in the shape of an anticyclonic gyre (Figs. 7a and 7b), and its time series (Fig. 7c) shows that there was a change from cyclonic to anticyclonic on 13 October; the whole process lasted $\sim$20 days.

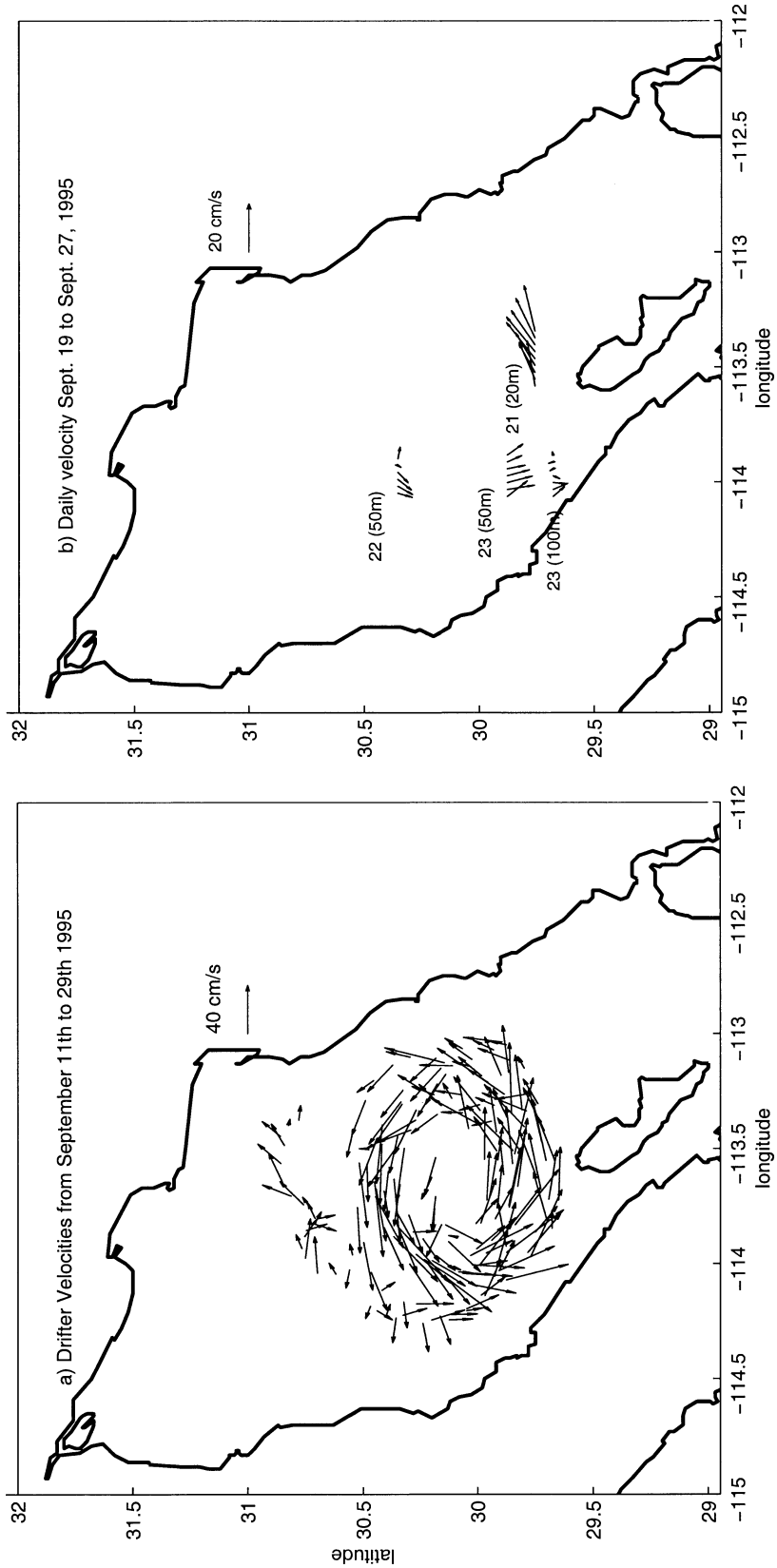

FIG. 4. (a) Drifter velocities for the 1995 cyclonic period. (b) Current meter velocities for the 1995 cyclonic period. (Only current meter at mooring 21 began on 19 Sep; other moorings began 2 or 3 days later.) The number in parenthesis indicates the depth of the current meter. Note: velocity scales are different in (a) and (b).

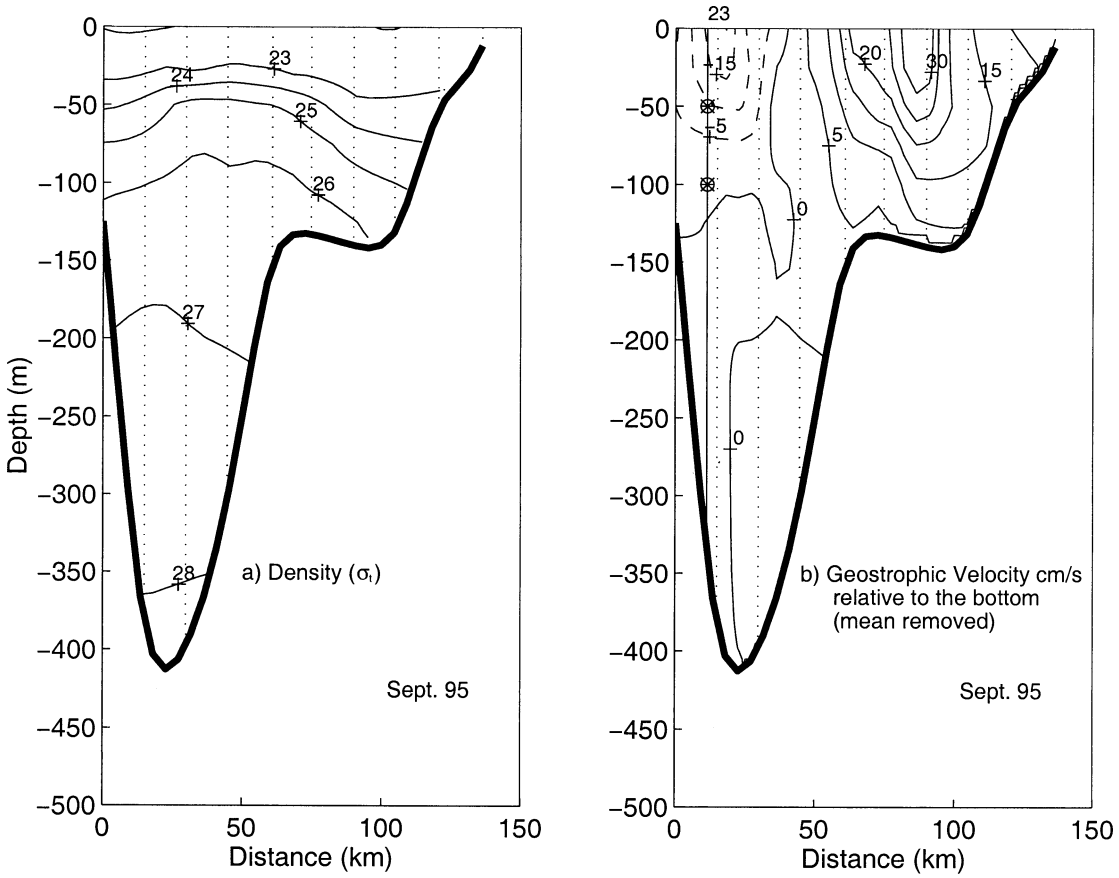

FIG. 5. Data from survey FU9509: vertical sections along the line shown in Fig. 2c (dotted lines indicate CTD stations). (a) Density (σ_t) and (b) geostrophic velocity; position of current meters shown by symbol ⊛.

The drifter velocities during the transition period are shown in Fig. 8; these data are a direct continuation of those in Fig. 4a, which contain the cyclonic gyre. From 30 September to 8 October 1995 (Fig. 8a), the magenta drifter traced a little anticyclonic gyre (~0.30 m s^{-1}), while the other drifters suggest a cyclonic gyre, smaller and weaker than that in Fig. 4a; at the end of the period, the blue and green drifters moved to the south over the mainland shelf. From 8 to 17 October (Fig. 8b) all the drifters moved slowly (~0.10 m s^{-1}); then, from 17 October to 4 November, the green and magenta drifters followed an anticyclonic path. The red drifter remained to the east of Ángel de la Guarda Island for most of the period, moving erratically and slowly, before running aground.

c. Anticyclonic regime

1) OCTOBER 1995–APRIL 1996

The current meter data shown in Fig. 6 provided very good spatial and temporal coverage of almost all of the 1995–96 anticyclonic period. The near-surface currents are quite variable, especially in the east (Fig. 6d; for position of the moorings see Fig. 2f) and south (Fig. 6g); currents to the west (Fig. 6b) and north (Fig. 6a) are stronger (~0.35 m s^{-1}) and more persistent, particularly in December and January. In Figs. 9a,b, each vector represents a 15-day average taken from the low-passed data shown in Fig. 6. The upper-layer low-passed currents (Fig. 9a) show a clear anticyclonic circulation with a mean velocity of ~0.20 m s^{-1}. The corresponding data for the deeper layers (85 and 100 m; Fig. 9b) show lower speeds (~0.10 m s^{-1}). Defining the depth of the gyre at site 23 as the depth where the current becomes zero before changing direction, it is estimated, by linear extrapolation, to be ~140 m. This is deeper than the cyclonic gyre.

The drifters were repositioned in the central NGC on 26 February 1996. They followed an anticyclonic path with mean velocities ~0.40 m s^{-1} (Fig. 10) until early April. The exception was the south drifter (indicated in the legend), which remained between the two large islands throughout the winter; it moved around just north of Tiburón Island until it was recovered on 17 March 1996. The gyre velocity measured by the drifters (Fig. 10) is about 40% higher than the current meter velocities, which is probably due to the deeper position of the current meters; as shown above, the current meters registered a strong vertical shear (0.0011 s^{-1}).

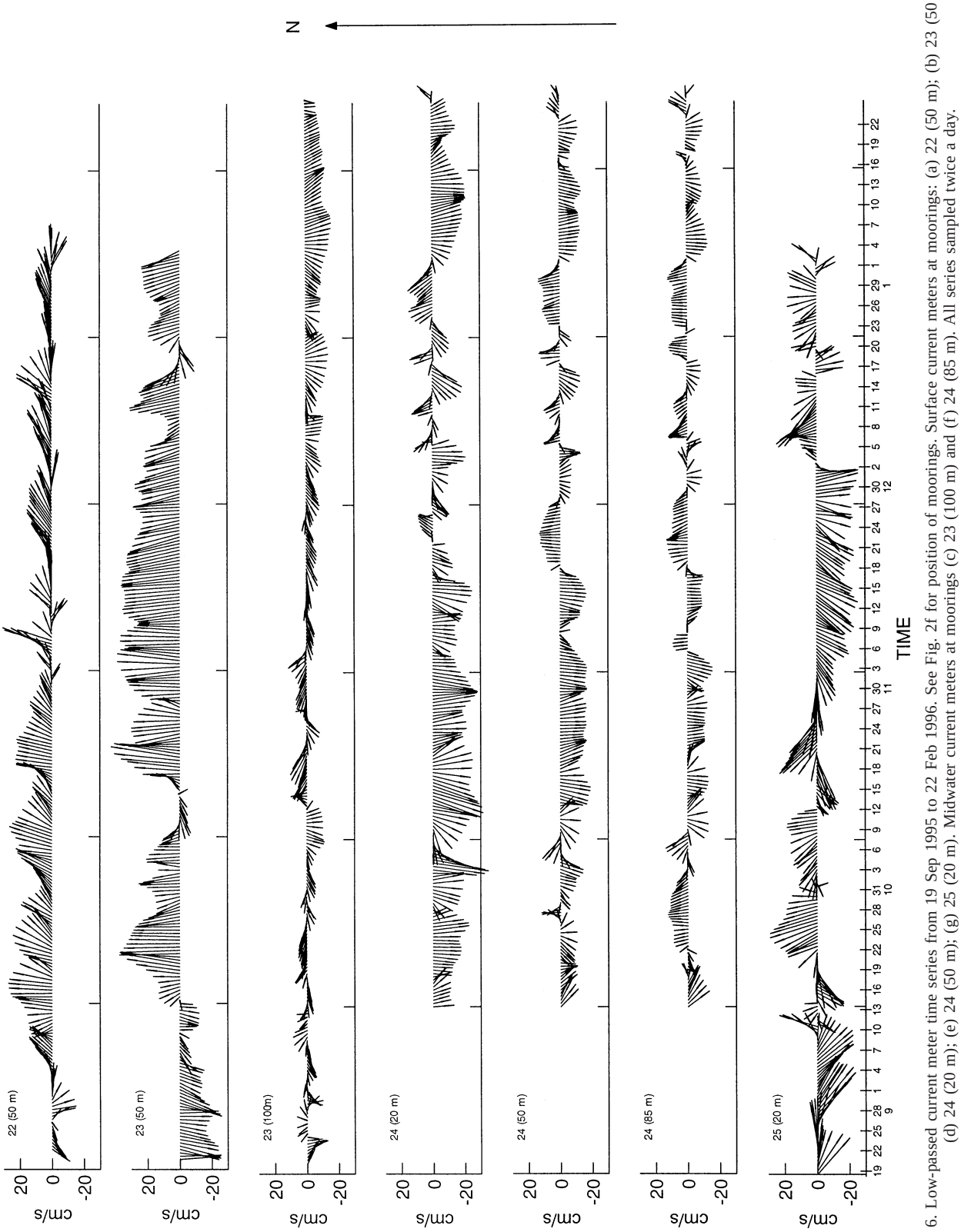

FIG. 6. Low-passed current meter time series from 19 Sep 1995 to 22 Feb 1996. See Fig. 2f for position of moorings. Surface current meters at moorings: (a) 22 (50 m); (b) 23 (50 m); (d) 24 (20 m); (e) 24 (50 m); (g) 25 (20 m). Midwater current meters at moorings (c) 23 (100 m) and (f) 24 (85 m). All series sampled twice a day.

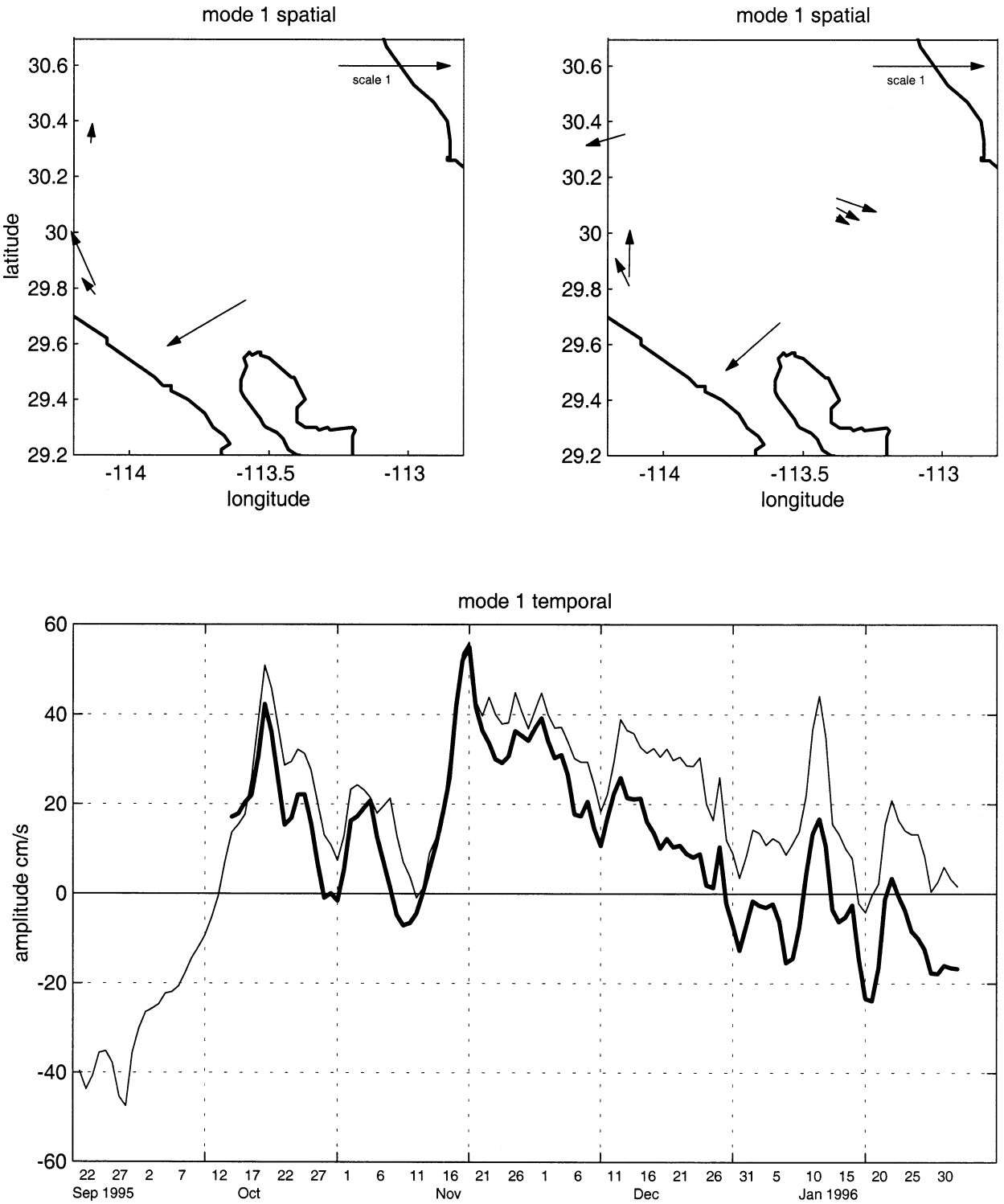

FIG. 7. First EOF mode of the current meter time series. (a) Space distribution, not including mooring 24. (b) Space distribution, including mooring 24. (c) Temporal signal: thin line not including mooring 24; bold line including mooring 24.

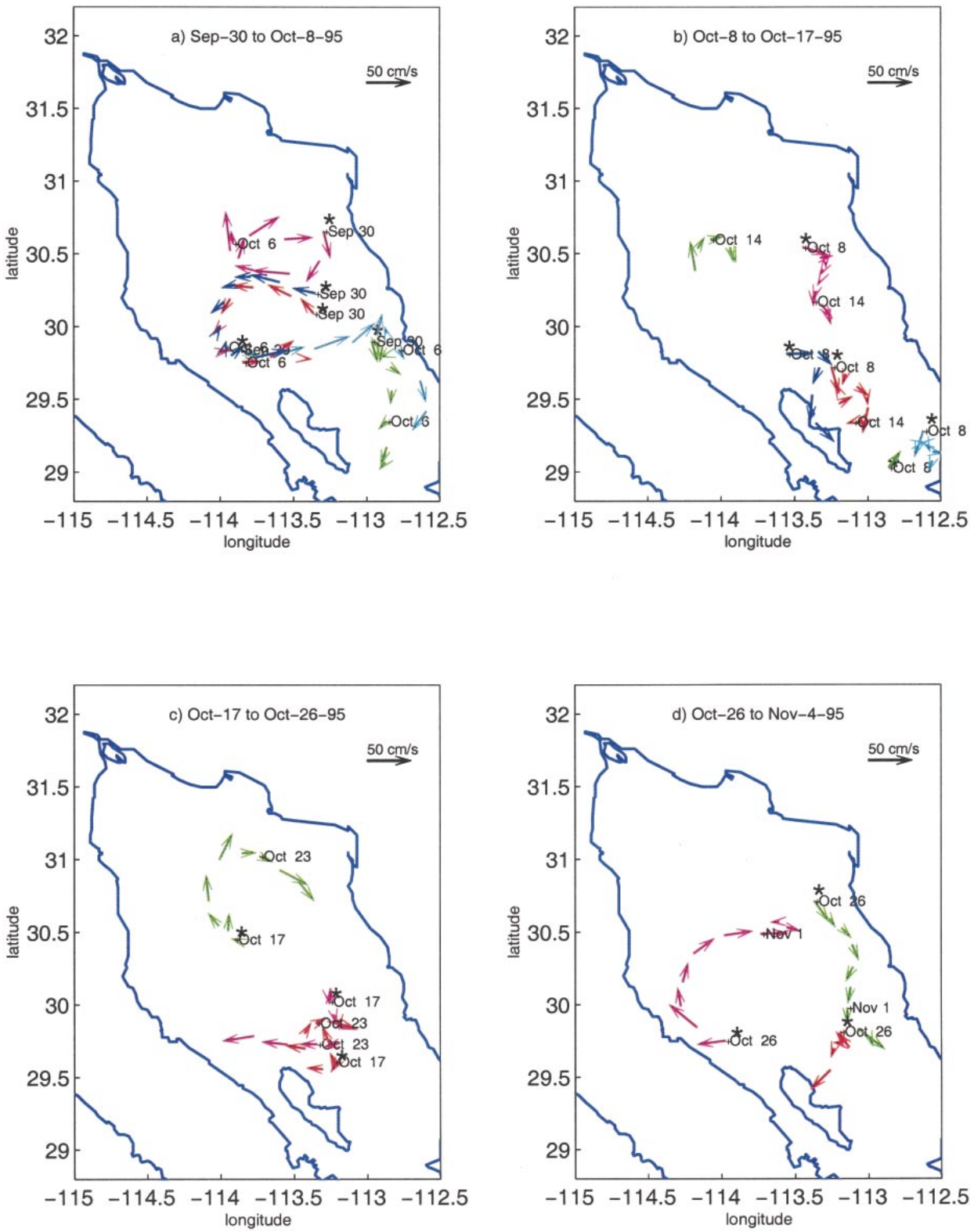

FIG. 8. 1995 autumn transition observed by drifters.

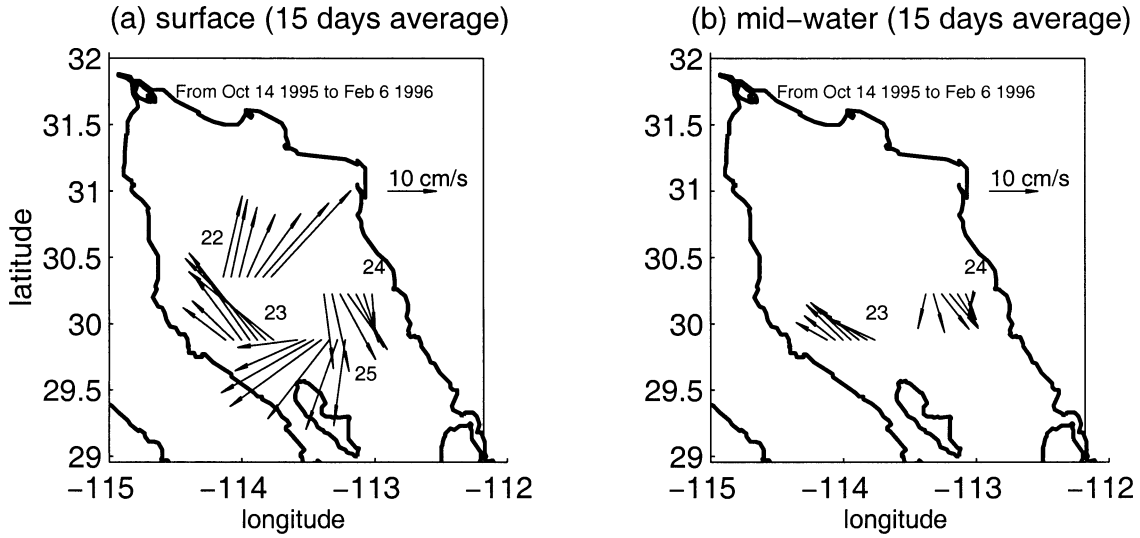

FIG. 9. 1995–96 anticyclonic period observed by current meters: (a) surface current meters; (b) midwater current meters. Each vector represents a 15-day average of the data shown in Fig. 6.

A hydrographic survey took place near the end of the anticyclonic period (25 March–9 April; Fig. 11), 30 days after the end of the current meter data presented in Fig. 6 but with the drifters still in operation. Stratification, as measured by Φ, had decreased considerably to $\sim$100 J m^{-3} (Fig. 11a). The geostrophic currents (Fig. 11b) are only $\sim$0.10 m s^{-1}, which is only 25% that of the drifters. This was noted by Lavín et al. (1997), who interpreted it as evidence that the gyre was partly barotropic and partly baroclinic. This proposition is supported by the numerical model of Beier and Ripa (1999), who find that the barotropicity is due to the interaction of the flow with the coast and the bathymetry.

2) DECEMBER 1994 DATA

Current meter and CTD data pertaining to the early stages of the anticyclonic regime were obtained in December 1994; they are presented here as a complement to the data just shown, which were representative of the later stages. In addition, they are the only simultaneous observations of currents and hydrography for this regime.

Stratification in December 1994 produced values of Φ $\sim$200 J m^{-3} in the deeper areas of the NGC (Fig. 11c), which is some 100 J m^{-3} higher than in March 1996 (Fig. 11a). The geostrophic currents (Fig. 11d) showed an anticyclonic gyre somewhat to the northwest of the position of the summer gyre, with currents of $\sim$0.20 m s^{-1}, which is twice the mean value in March 1996. This shows, in agreement with the description of the seasonal behavior of Φ (Organista 1987; Argote et al. 1995) and of geostrophic velocity (Bray 1988; Carrillo et al. 2001), that both stratification and geostrophic velocities were stronger in December 1994 than in March 1996.

The low-passed surface (20–38 m) current meter data for the period 29 November–28 December 1994 (Figs. 12a and 12b) show the anticyclonic gyre, with the strongest currents to the west and north. Mooring 5 is outside the gyre and therefore it does not follow the pattern of the other instruments. The measured surface speeds ($\sim$0.20 m s^{-1}) are similar to the geostrophic ones. The current meter data for the two December surveys (Figs. 6a–g and 12a,b) show surface speeds of similar magnitude, $\sim$0.20 m s^{-1}.

The current meter data from a depth of 120 m (Figs. 12e and 12f) also show anticyclonic circulation, but not as clearly as in the shallower level; in fact, there are direction reversals at moorings 2 and 3. On mooring 6 there was a current meter at 197 m; the currents measured there have a $\sim$180° deviation from the shallower current meters, indicating that the gyre has a baroclinic component. A time average was made for all the time series at this mooring, and linear interpolation was used to make a gross estimate of the depth of the gyre, obtaining $\sim$130 m. The vertical structure of density and geostrophic velocity at cross sections A and B (see positions in Fig. 2a) where the instruments were located (Fig. 13) shows the concavity of the isopycnals and the zero of the currents at a depth of $\sim$150 m and in the entire water column in the center of the gyres.

d. Spring transition (from anticyclonic to cyclonic)

The spring transition is expected to occur in April or May (Carrillo et al. 2001). Data pertaining to this transition are the drifter time series from 5 April to 8 July 1996. Unfortunately no current meter data were avail-

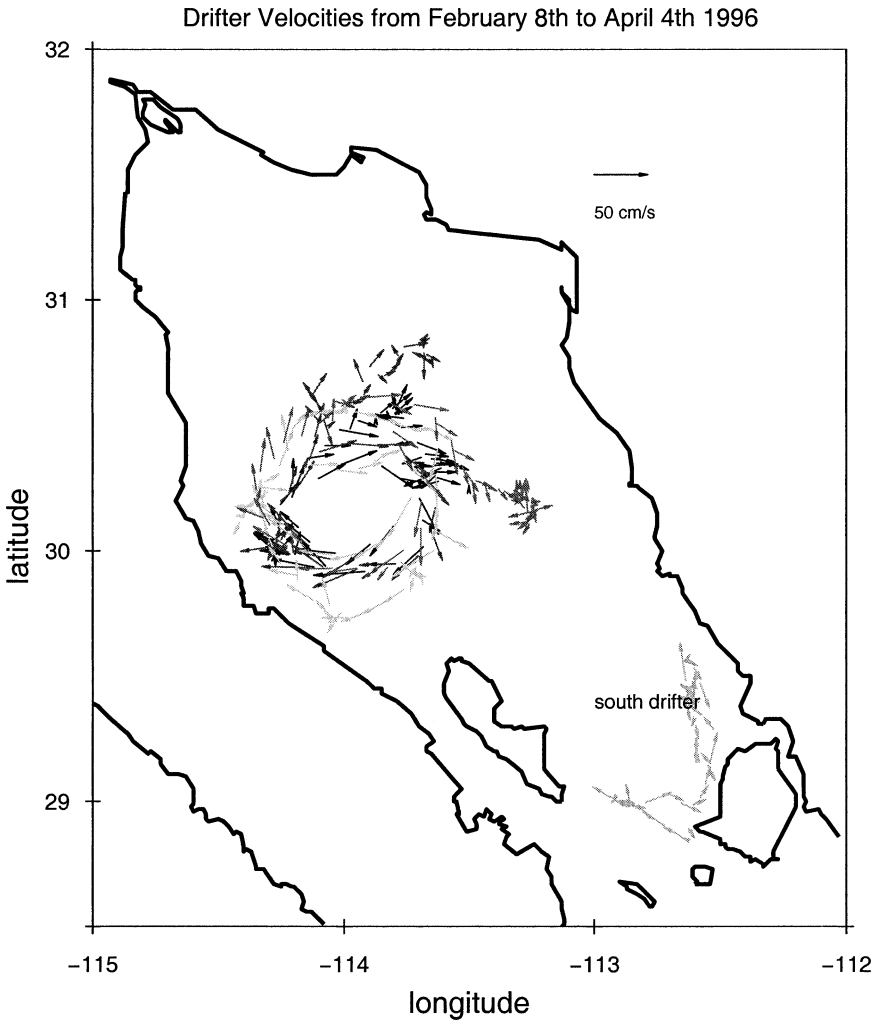

FIG. 10. Drifter velocities for the 1995–96 anticyclonic period (the position of the south drifter is indicated by legend).

able for this transition, nor indeed concurrent hydrographic data.

Trajectories and velocities of the two only surviving drifters from 5 to 28 April 1996 are shown in Fig. 14a, which are a continuation of those shown in Fig. 10. From 5 to 15 April (Fig. 14a) the black drifter suggests the relics of the anticyclonic circulation, while the gray drifter shows almost no motion. On 15 April (Fig. 14a) the black drifter stops abruptly and moves very little for almost a month: on 13 May (Fig. 14b), both drifters began to move and soon were following a cyclonic path. The drifters seem to have followed the outer edge of a cyclonic gyre covering the whole NGC (twice for the black drifter!) until the end of the time series (Figs. 14c,d). According to these data, the transition took about one month.

4. The ocean model

The model used here is a nonlinear, entraining version of the inhomogeneous-layer model in primitive equations used by B97. The simulation was started from rest and a state of equilibrium was reached after 15 years. The model consists of two active layers of fluid on top of a rigid bottom $z = h_0(x, y)$. The surface and bottom layer thicknesses are $h_1(x, y, t)$ and $h_2(x, y, t)$, respectively. The temperature of the surface layer is $T_1(x, y, t)$, while the bottom layer has a constant and homogeneous temperature T_2. Coordinate x extends roughly southeastward along the gulf, from 0 at the head increasing toward the mouth. Coordinate y extends roughly northeastward across the gulf, from 0 at the Peninsula of Baja California, increasing toward the mainland. Although the model is applied to the whole Gulf of California (Beier 1999), only the results for the NGC are analyzed here. The mass conservation equations are

$$\frac{\partial h_i}{\partial t} + \nabla \cdot (h_i \mathbf{u}_i) = (-1)^{i+1} w_e,$$

where $i = 1,2$ is the layer index and $\mathbf{u}_i = (u_i, v_i)$, and

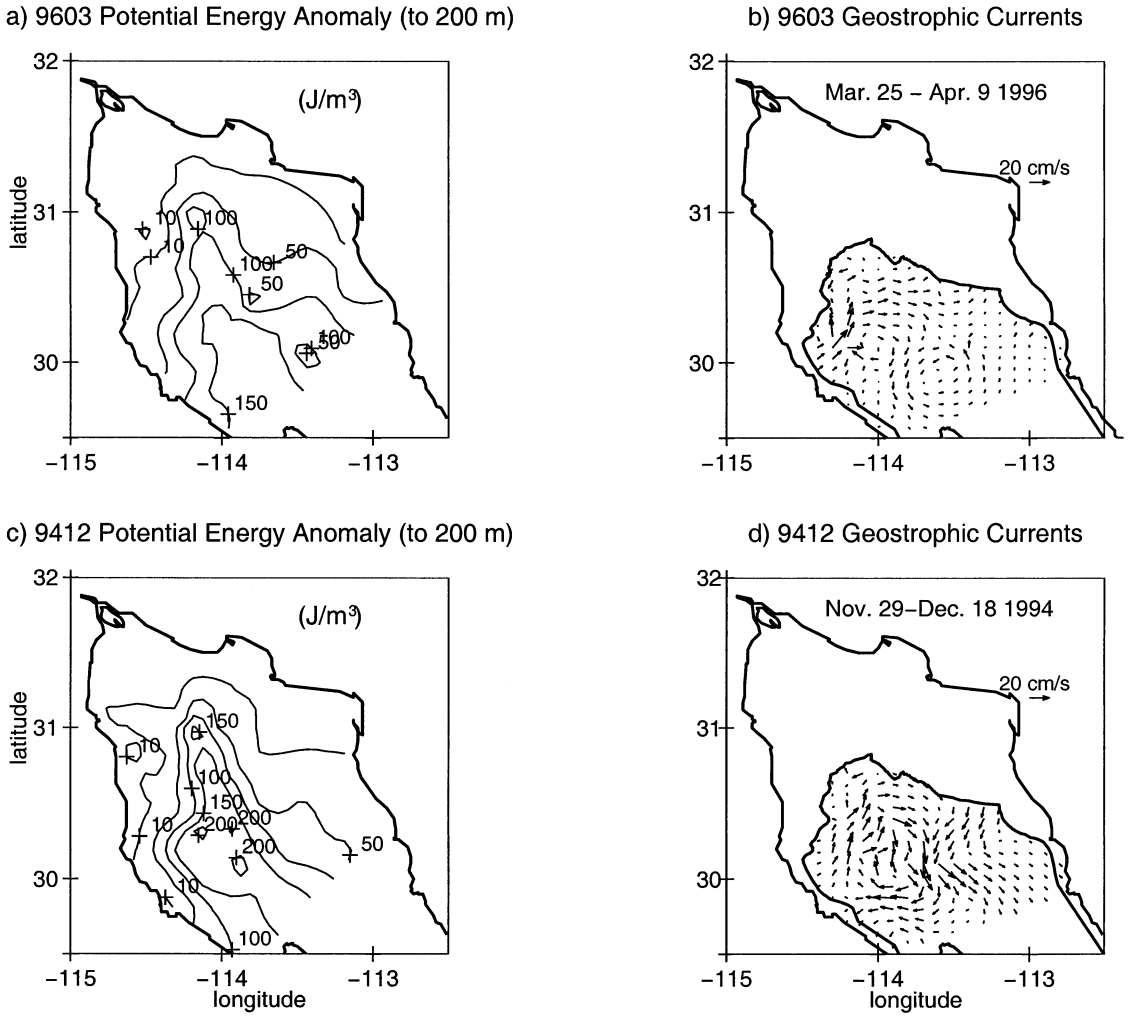

FIG. 11. (a) Potential energy anomaly Φ (to 200 m) and (b) geostrophic velocities (10 m referred to 100 m) for the FU9603 campaign. (c) and (d) As above but for the FU9412 campaign. (The 100 m isobath is indicated.)

w_e is the entrainment velocity. The nonlinear equations of motion are

$$\frac{D\mathbf{u}_1}{Dt} + f\mathbf{k}\times\mathbf{u}_1 + \langle\nabla p_1\rangle = \mu\nabla^2\mathbf{u}_1 + \frac{\boldsymbol{\tau}}{h_1\rho_0} + w_e(\mathbf{u}_2 - \mathbf{u}_1)/h_1,$$

$$\frac{D\mathbf{u}_2}{Dt} + f\mathbf{k}\times\mathbf{u}_2 + \langle\nabla p_2\rangle = \mu\nabla^2\mathbf{u}_2 - C_D\frac{\mathbf{u}_2(u_2^2 + v_2^2)^{1/2}}{h_2},$$

where $f(x, y)$ is the Coriolis parameter (7.51×10^{-5} s^{-1}), μ is the horizontal eddy viscosity (30 $m^2\ s^{-1}$), $C_D = 4.4 \times 10^{-3}$ is the drag coefficient, and the vertical averages of the pressure gradients are

$$\langle\nabla p_1\rangle = \theta_1\nabla(h_0 + h_1 + h_2) - \left(h_0 + \frac{h_1}{2} + h_2\right)\nabla\theta_1$$

$$\langle\nabla p_2\rangle = \nabla[\theta_1 h_1 + \theta_2(h_0 + h_2)],$$

where $\theta_i = g\rho_i/\rho_0$ is the buoyancy of the layers and ρ_0 is a constant density used in the Boussinesq approximation,

$$\rho_1 = \rho_0[1 - \alpha(T_1(x, y, t) - T_0)],$$

$$\rho_2 = \rho_0[1 - \alpha(T_2 - T_0)],$$

where $\alpha = 2.4 \times 10^{-4}\ K^{-1}$ and T_0 is the reference temperature. The heat conservation equation of the upper layer is

$$\frac{DT_1}{Dt} - \frac{H_1}{h_1}\mu\nabla^2 T_1 - \frac{Q_s}{\rho c_p h_1} = \varepsilon(x)(T_b - T_1) - w_e\frac{(T_1 - T_2)}{h_1}, \qquad (1)$$

where the terms on the left represent the material derivative, heat diffusion, and the surface heat flux, respectively. The first term on the right is a sponge term applied only in the open boundary at the mouth of the gulf; T_b is the (constant and homogenous) observed

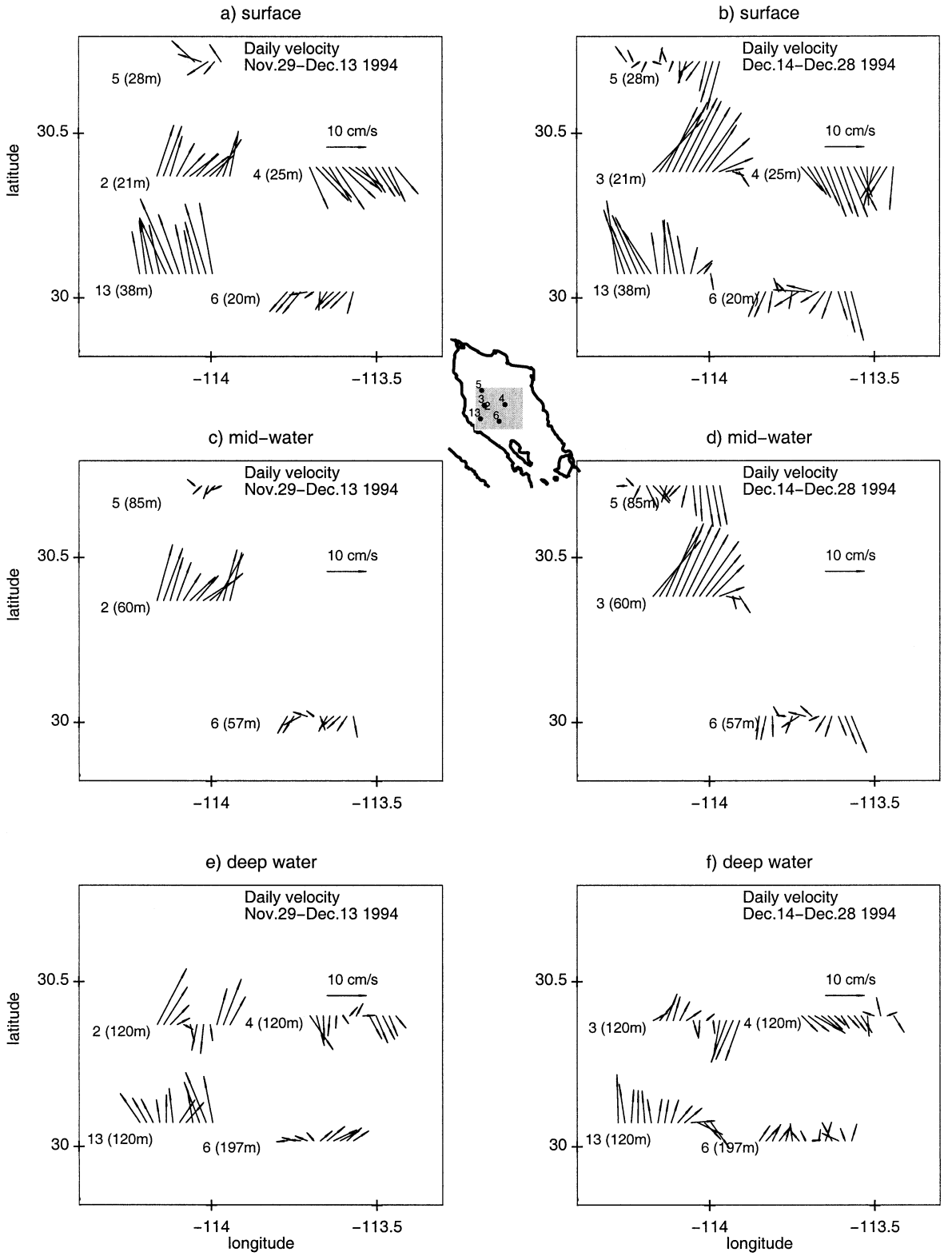

FIG. 12. Dec 1994 anticyclonic period shown by low-passed current meter data (sampled daily). Mooring positions in the central insert map. (a) Surface from 29 Nov to 13 Dec. (b) Surface from 14 to 28 Dec. (c) Midwater from 29 Nov to 13 Dec. (d) Midwater from 14 to 28 Dec. (e) Deep water from 29 Nov to 13 Dec. (f) Deep water from 14 to 28 Dec.

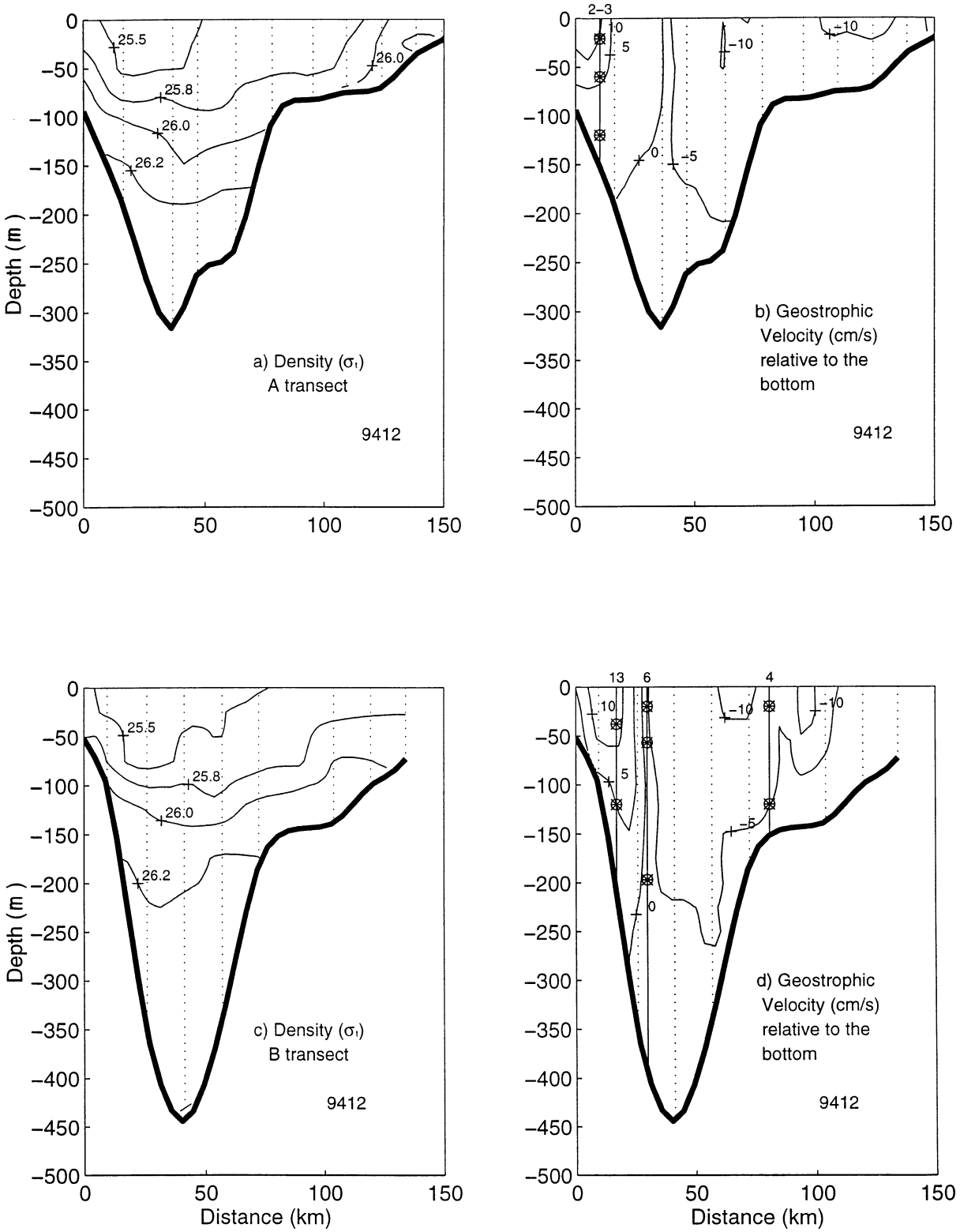

FIG. 13. Vertical cross sections for the FU9412 campaign along lines of stations shown in Fig. 2a: (a) density (σ_t) and (b) geostrophic velocity and mooring and current meters positions for transect A; (c) density (σ_t) and (d) geostrophic velocity and mooring and current meters positions for the transect B. In the four figures, dotted lines indicate CTD stations.

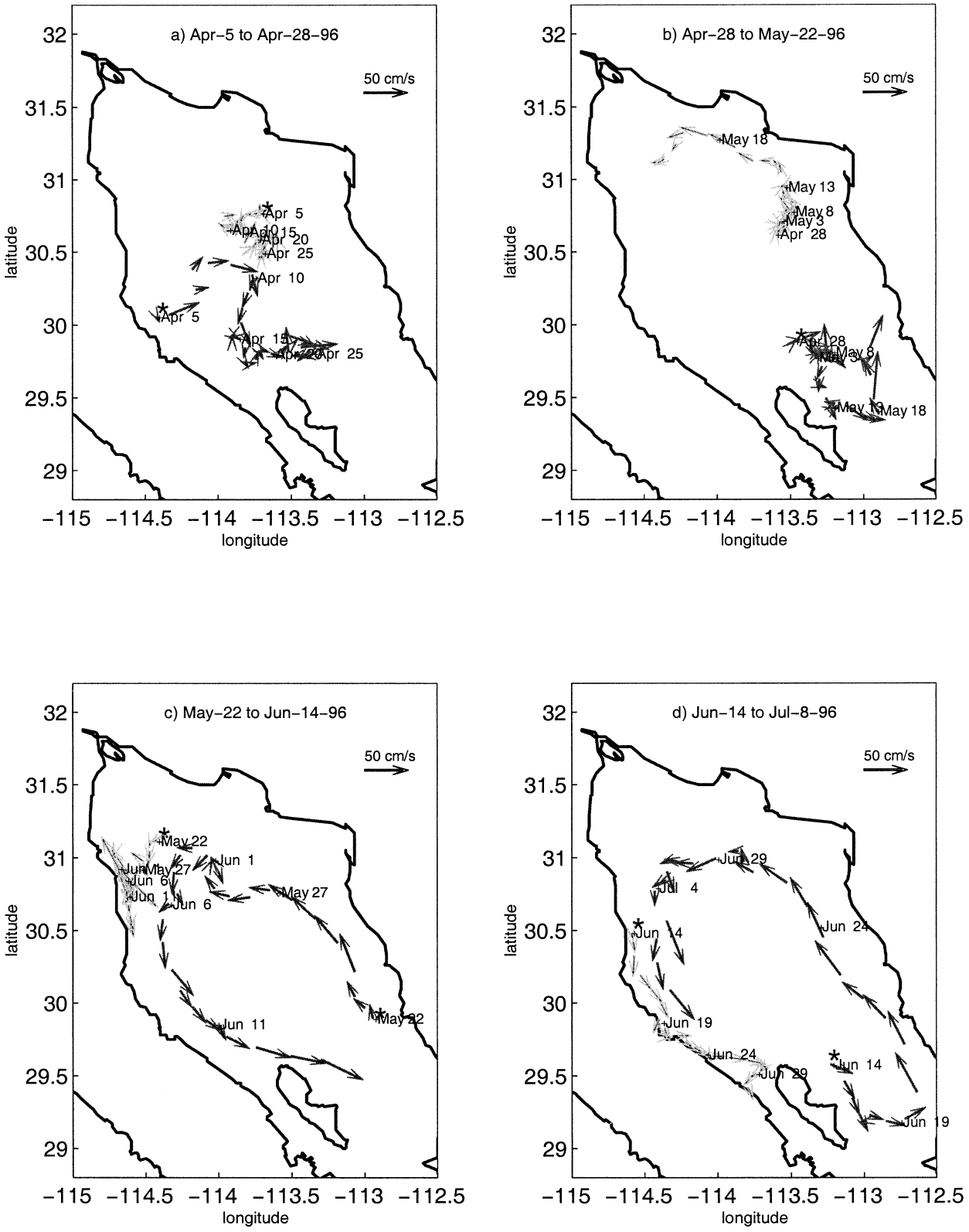

FIG. 14. 1996 spring transition observed by drifters.

mouth temperature obtained from the hydrographic historical observations. The second term on the right represents the effect that the temperature of the entrained water has upon the heat content of the surface layer. Heat flux normal to the coast is zero.

The entrainment velocity w_e is parametrized following McCreary et al. (1991):

$$w_e = \begin{cases} \dfrac{(h_1 - H_e)^2}{H_e t_e}, & h_1 \le H_e \\ 0, & h_1 > H_e, \end{cases} \quad (2)$$

where H_e and t_e characterize the entrainment process. Entrainment acts as a process that prevents the interface from surfacing, incorporating water from the bottom layer to the surface layer, thus cooling and slowing down the surface layer. According to Eq. (2), the entrainment acts when $h_1 \le H_e$ and increases parabolically to a maximum value of H_e/t_e. Entrainment is a selective process that acts during winter in the NGC when the interface moves toward the surface, driven by the external forcing mechanisms of the circulation (B97).

The chosen values, $H_e = 55$ m and $t_e = 2$ days, are typical of those used to simulate the entrainment process in layered models. For example, McCreary et al. (1989) used $t_e = 0.8$ days, McCreary et al. (1991) used $t_e = 0.5$ days, and Lu et al. (1998) used $t_e = 5$ days. The entrainment timescale t_e must be chosen small enough to ensure that the interface does not surface in regions of intense upwelling; otherwise solutions are not particularly sensitive to its value (McCreary and Kundu 1988; McCreary et al. 1989). However, solutions are sensitive to the value of H_e. McCreary et al. (1989) used $H_e = H_1 = 50$ m, where H_1 is the initial value of the surface layer; however, in our case of the Gulf of California, a value of H_e equal to the initial value of the thickness of model surface layer ($H_1 = 70$ m) causes the elimination of the summer cyclonic circulation, which would be in serious disagreement with observations. More realistic results are obtained by choosing a value of H_e close to the average depth of the surface mixed layer, which, according to Martínez-Sepúlveda (1994), varies between a few meters in summer to about 90 m in winter. The chosen value ($H_e = 55$ m) produced the best surface temperature simulation as compared to observations (see below).

The model uses the same forcing agents as in B97 with the addition of a net average heat input at the surface Q_o. The surface heat flux is therefore given by $Q_s = Q_o + A(x, y)\cos(\omega t + \phi)$, where Q_o has a constant value along the gulf and $A(x, y)$ and $\phi(x, y)$ are the observed (Castro et al. 1994) amplitude and phase of the annual surface heating. The amplitude has a maximum around the central archipelago and diminishes toward both the mouth and the head of the gulf (Paden et al. 1991; Castro et al. 1994; Berón-Vera and Ripa 2000). In the annual average, the Gulf of California gains heat through the surface at a rate of $Q_o \times$ (area of the gulf) = 18 TW (TW = 10^{12}W), which has to exit through the mouth in order to achieve balance.

The internal processes involved in this balance are still unknown; many different temporal scales could be responsible for these important interchanges with the atmosphere and the Pacific Ocean. However, in the annual average and if diffusion is not considered, Eq. (1) results in an upper-layer heat balance between Q_o and the temporal average of both the entrainment term and the horizontal advection of heat:

$$Q_0 = \langle \rho C_p w_e (T_1 - T_2) \rangle + \langle \rho C_p h_1 (\mathbf{u}_1 \cdot \boldsymbol{\nabla}) T_1 \rangle. \quad (3)$$

However, if the total value of Q_o is used in the model as surface heat forcing, the mean surface temperature obtained increases monotonically toward the head, which is in disagreement with the observation that the mean surface temperature of the gulf decreases from the mouth to the archipelago and then increase slightly toward the head (Soto-Mardones et al. 1999). Therefore, a value of Q_o was used that gives a mean surface temperature in agreement with the observations; for $H_e =$ 55 m and $t_e = 2$ days a value of $Q_o = 7$ TW is needed in order to obtain realistic surface temperatures. It is likely that the full 18 TW could be used by adjusting the values of H_e and t_e, but it was decided not to do this, the main purpose of the numerical experiments being to illustrate the effects of entrainment on the seasonally reversing circulation of the NGC. Tidal mixing is not included in the model; it is very important in the NGC (Argote et al. 1995) and its inclusion could allow a higher value of Q_o to be used (Beier 1999). An additional justification of the value of Q_o, used is that there are large uncertainties in its estimate (Lavín and Organista 1988; Castro et al. 1994; Berón-Vera and Ripa 2000).

Model results

1) SEA LEVEL AND SURFACE TEMPERATURE

In order to highlight the effect of entrainment on the seasonal circulation in the NGC, three versions of the model are compared: linear (B97), nonlinear, and nonlinear with entrainment.

Figure 15 shows the observed amplitudes and phases of the annual signal of sea level along the gulf's mainland and peninsular coasts, together with those simulated by the nonlinear entraining model. In the NGC the nonlinear model with entrainment performs better than the linear model of B97 (cf. his Fig. 14 against our Fig. 15). The nonlinear model without entrainment produces results very similar to those of the linear model of B97. Therefore, the intense entrainment in the NGC results in a sea level amplitude that is ~2 cm smaller than for the model of B97, and more in accord with the observations.

In Fig. 16, the transversely averaged annual mean, amplitudes, and phases of T_1 simulated by the three

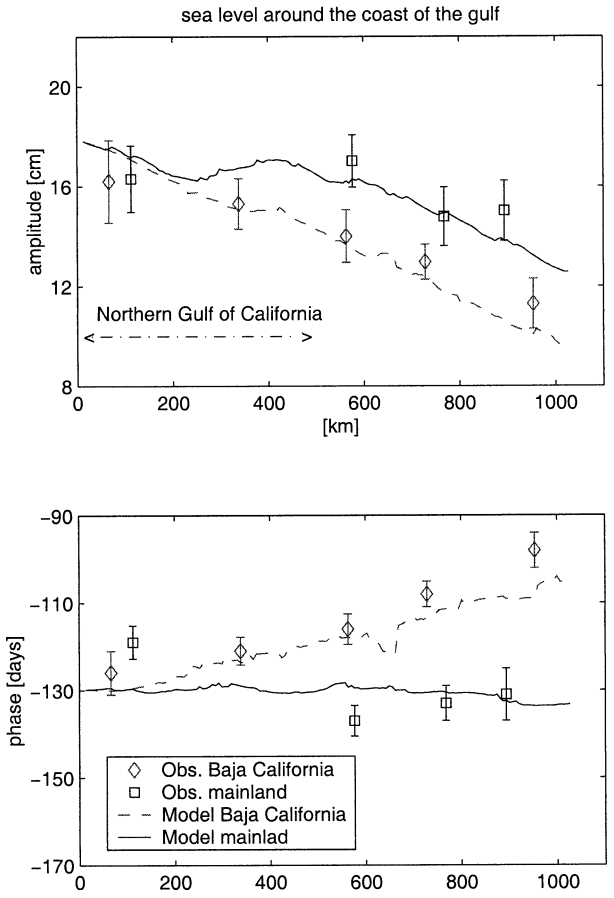

FIG. 15. Comparison between sea level height at the annual frequency obtained with the nonlinear entraining model and observations (symbols) as a function of distance from the head of the gulf. (a) Amplitudes (m). (b) Phases (days).

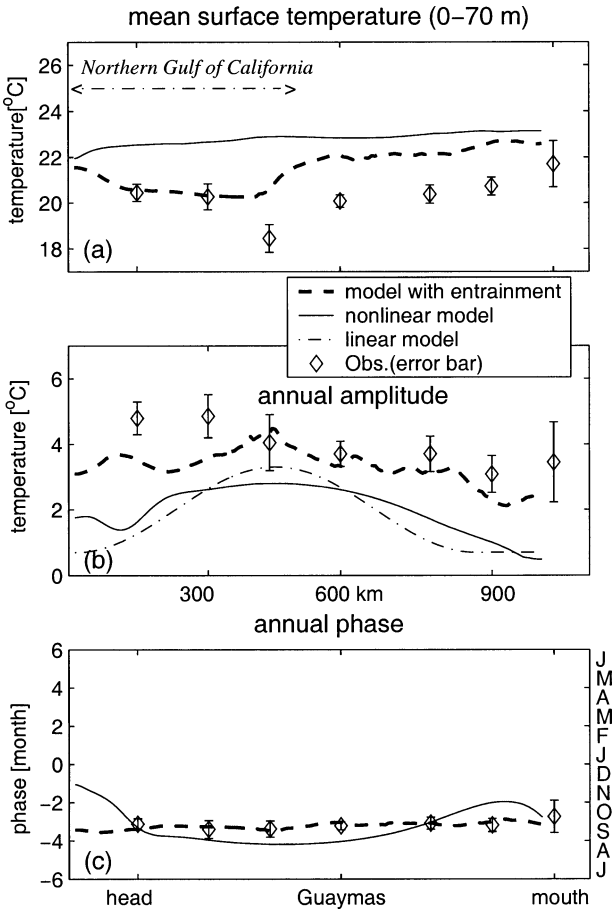

FIG. 16. Comparison of observed and simulated sea surface temperature annual harmonics, as a function of distance from the head of the gulf. Symbols: observed mean temperature of the top 70 m (T_{70}). Lines: transversely integrated simulated sea surface temperature obtained with the different versions of the model. Dot–dash, linear model; thin line, nonlinear model without entrainment; bold dashed line, nonlinear entraining model. (a) Mean temperature. (b) Annual amplitude. (c) Phase.

versions of the model are compared against the same quantities for T_{70} (from Berón-Vera and Ripa 2000). The annual mean of T_{70} decreases from the mouth to the head, with a minimum in the archipelago (Fig. 16a), a feature reproduced only by the model with entrainment. The observed annual amplitude of T_{70} (symbols in Fig. 16b) increases from the mouth to the head of the gulf; all the models reproduce qualitatively this behavior, but the model with entrainment shows better quantitative agreement. This is because entrainment cools the temperature of the surface layer, causing a larger annual variability, which is closer to the observations. The observed and simulated phases are all in good agreement (Fig. 16c).

The performance of the nonlinear entraining model goes beyond these comparisons: in order to satisfy the heat balance (3), both nonlinearity and entrainment are necessary. A stationary residual flow is necessary to export Q_o, and for such a residual flow to occur the advective terms must be included. As will be shown below, the stationary velocity appears in the model because of entrainment, through the continuity equation. Therefore, only the circulation simulated by the fully nonlinear model is shown in detail.

2) CIRCULATION

In order to compare the simulated circulation against the observed current measurements, a year of the instantaneous fields of the surface velocities produced by the nonlinear, entraining model is presented in Figs. 17–20; they clearly show cyclonic and anticyclonic periods of unequal length and shorter transitions periods than in the linear-model simulations of Beier and Ripa (1999).

The circulation of the surface layer from 30 December to 30 March (Fig. 17), shows an anticyclonic gyre covering most of the NGC. There is a coastal jet on the shelf of the continental side that carries surface water out of the NGC; in Ballenas-Salsipuedes Channel the

flow is into the NGC. The winter gyre seems to affect part of the head of the NGC and the shelf on the continental side.

Figure 18 shows the surface velocities during the transition period from winter to spring every 15 days. (Note the change of velocity scale with respect to Fig. 17.) The transition from anticyclonic to cyclonic circulation occurs between the end of April and the first half of May, which is in agreement with the direct observations. At the end of April the anticyclonic gyre has contracted and moved to Delfín Basin, while surface water starts to flow into the NGC off Tiburón Island; this incoming water becomes a coastal jet by mid-May and initiates the formation of a the basinwide cyclonic gyre. By 30 May the fully developed cyclonic gyre covers the entire NGC. In Ballenas Channel the flow is to the southeast from mid-May, as a branch of the overall cyclonic circulation.

From 30 June to 30 August the cyclonic gyre is located in the center of the NGC (Fig. 19), having contracted somewhat and moved to Delfín Basin. The flow in Ballenas–Salsipuedes Channel is very weak, while the coastal-jet flow into the NGC off Tiburón Island disappears sometime in August. At the end of September the cyclonic gyre is very weak but it is still located in the central part of the NGC.

The transition period from the summer cyclonic circulation to the winter anticyclonic circulation occurs between the end of September (Fig. 19d) and mid-October (Fig. 20a); the subsequent development of the circulation is presented every 15 days in Fig. 20. Although very weak, the anticyclonic gyre starts during the first half of October, as an outgoing coastal jet off Tiburón Island; by the end of the month it covers the entire NGC and by mid-November it is well defined and strong, reaching full development by the end of November.

The mean surface circulation (Fig. 21a), absent in the linear model of B97, consists of an elongated anticyclonic gyre with velocities of the order of 0.05 m s^{-1}, spanning the deeper parts of the NGC, including Ángel de la Guarda Island. There are a couple of smaller gyres: anticyclonic near the head and cyclonic in the middle of the gulf on the continental side. In the channels of the archipelago, the mean flow is out of the NGC, except in Ballenas Channel where it is toward the NGC. If entrainment is not included, the mean circulation becomes negligible, which means that the residual gyre and the two-layer exchange are both due to entrainment.

The mean position of the interface (Fig. 21b) shows negative values in the entire NGC due to the annual average of entrainment producing a net annual flux of water from the bottom layer to the surface layer. The thickness of the surface layer (80 m) is larger than that at rest state (70 m). The mean surface velocities follow the contours of the mean position of the interface, in geostrophic agreement with the sense of rotation of the main gyre. There is also a mean circulation ($^{-}0.1$ m s^{-1}) in the mainland shelf; this area is shallower than the surface layer, and therefore this flow is barotropic.

The amplitudes (Fig. 21c) and phases of the interface displacement (Fig. 21d) at the annual frequency indicate that maximum negative displacements occur in winter between February and March. These maximum values of the interface displacement are lower than those predicted by the linear simulations of B97 and Beier and Ripa (1999). The circular shape of the isolines in Figs. 21c,d represent the annual gyres, which when added to the annual mean circulation of Fig. 21a produce the asymmetric circulation shown in Figs. 17–20.

5. Comparison with the observed currents

In general, the seasonal circulation predicted by the model agrees very well with the observations. In the following paragraphs each circulation period is examined in some detail.

a. Cyclonic period

The model result corresponding to the August cruise (Fig. 3a) is Fig. 19b, while Fig. 19c corresponds to the 9–21 September cruise (Fig. 3b). The simulations that are to be compared with the drifter and current meter data are Figs. 19c,d with Figs. 4a,b. The qualitative agreement between model and observations is remarkable. Geostrophic currents and drifter velocities are 60% higher than the simulated ones, but there was a good agreement with the current meter speeds; the quantitative differences are not important, in view of the simplified vertical structure of the model. The model suggests that by 30 September (Fig. 19d) the summer circulation regime was coming to an end, and the direct observations concur, as shown below.

b. Autumn transition

The similarity between the numerical simulations and the observations during this transition is very good. The end of the cyclonic gyre in the model occurs between 30 September (Fig. 19d) and 15 October (Fig. 20a), corresponding to drifter data in Figs. 4a and 8a,b (30 Sep–17 Oct). In the model, the anticyclonic gyre starts as a jet between Tiburón and Ángel de la Guarda Islands (Fig. 20a), which would correspond to the blue and green trajectories in Fig. 8a. The model also presents a stagnation area east of Ángel de la Guarda Island (Figs. 20a,b), which may correspond with the behavior of the red drifter in Figs. 8b–d. Finally, the model shows a well-developed anticyclonic gyre by early November (Figs. 20b,c), in agreement with the green and magenta drifters in Fig. 8d.

c. Anticyclonic period

The numerical simulations (Fig. 17) show, in general, the same circulation pattern as the observations, and

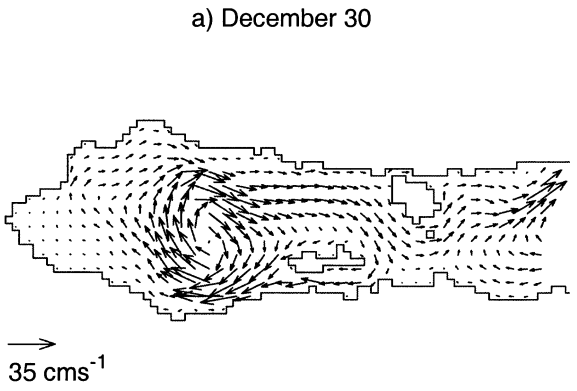

FIG. 17. Simulated anticyclonic circulation (a) 30 Dec; (b) 30 Jan; (c) 28 Feb; and (d) 30 Mar.

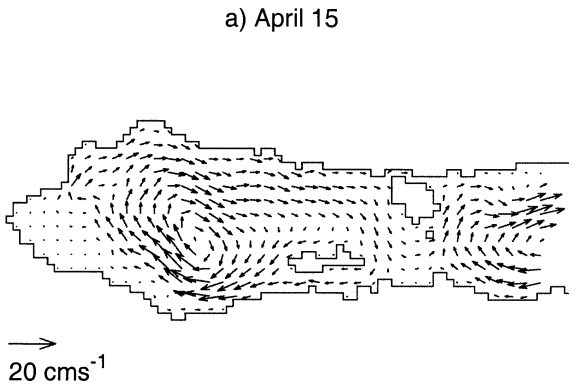

FIG. 18. Simulated spring transition (a) 15 Apr; (b) 30 Apr; (c) 15 May; and (d) 30 May.

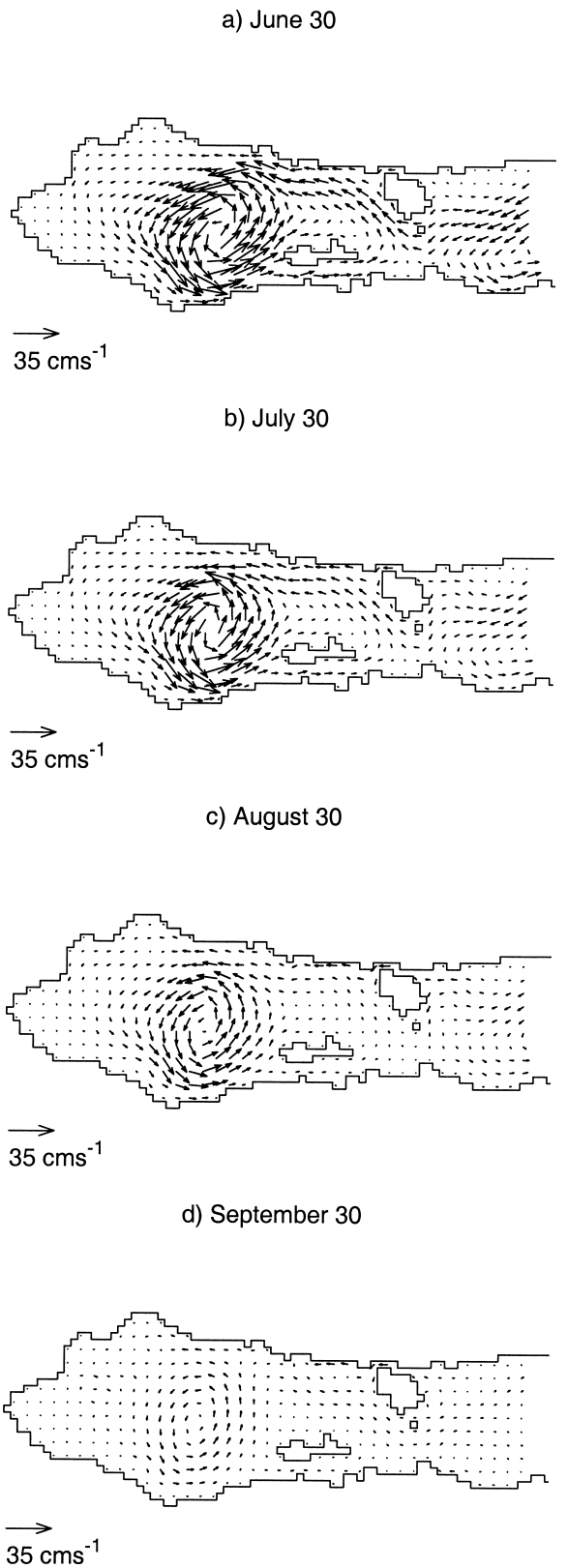

FIG. 19. Simulated cyclonic circulation (a) 30 Jun; (b) 30 Jul; (c) 30 Aug; and (d) 30 Sep.

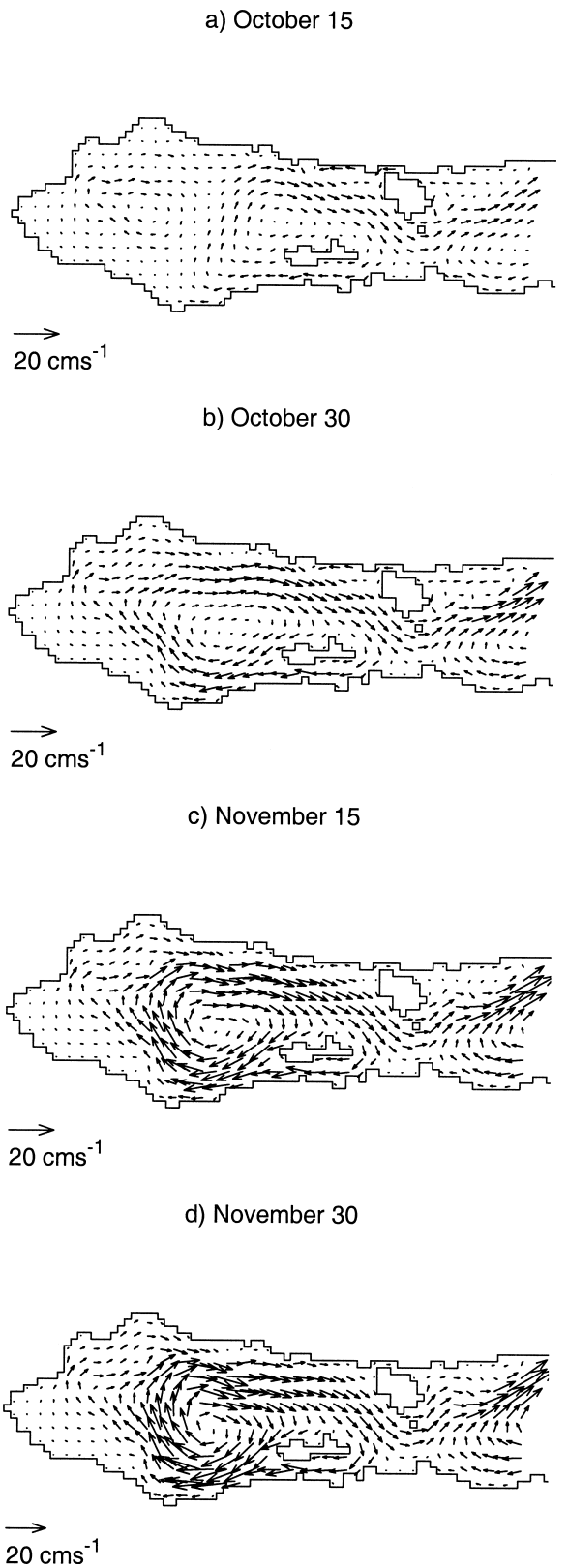

FIG. 20. Simulated autumn transition (a) 15 Oct; (b) 30 Oct; (c) 15 Nov; and (d) 30 Nov.

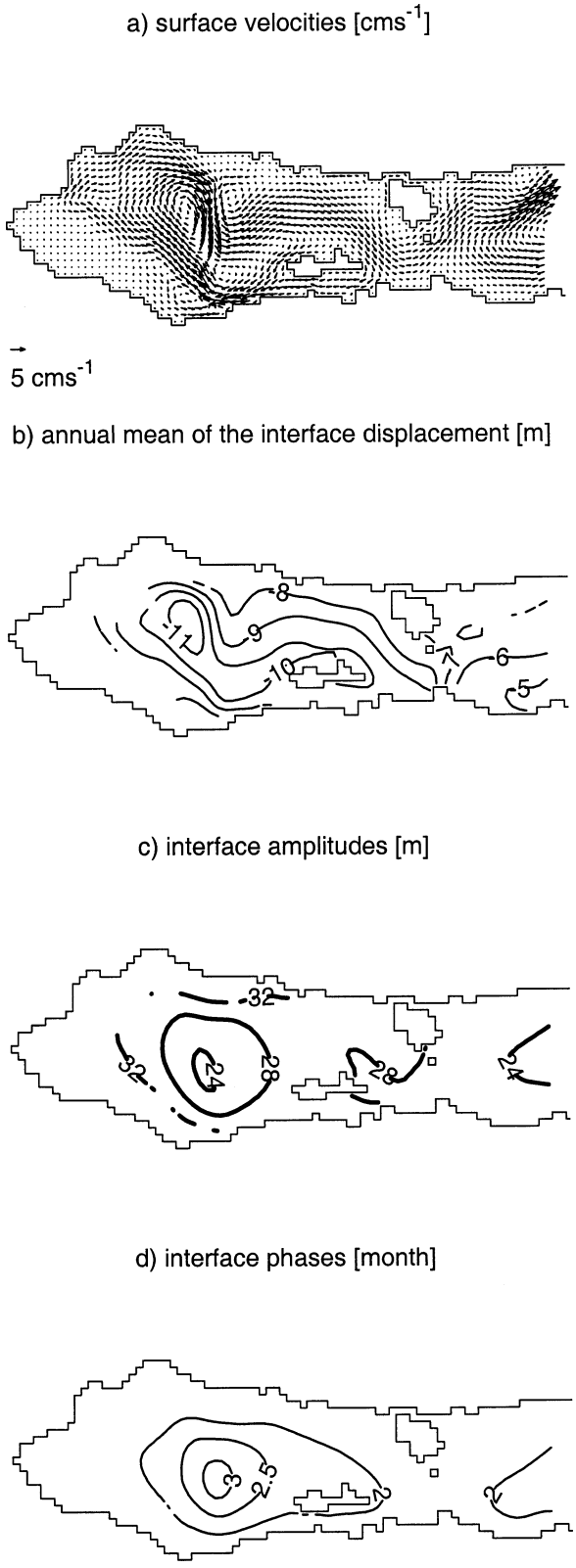

FIG. 21. Annual mean circulation predicted by the nonlinear model with entrainment. (a) Surface velocities (cm s^{-1}) and (b) annual mean interface displacement (m); (c) annual harmonics of interphase displacement amplitudes (m) and (d) phases (month).

there are other important agreements: the anticyclonic gyre lasts for about 6 months, and the current speeds are similar to those of the drifters and of the current meters ($\sim$0.30 m s^{-1}). As a comparison, the model without entrainment (B97) predicted a duration of $\sim$4 months and speeds of $\sim$0.65 m s^{-1}.

However, there are some discrepancies. The simulated gyre occupies almost the entire width of the NGC, while the observed gyre was found (both by drifters and current meters) only in areas where the bottom depth exceeded 100 m. Also, the south drifter suggests that currents to the north of Tiburón Island were variable in direction (Fig. 10), while the model predicts an outgoing jet.

d. Spring transition

The similarity between the model simulations (Fig. 18) and the drifter data (Fig. 14) is remarkable: little movement is predicted at the end of April (Fig. 18b), and by 15 May the circulation has started as a coastal jet on the mainland shelf (Fig. 18c). The speeds differ by 50% (drifters $\sim$0.20 m s^{-1}; model $\sim$0.10 m s^{-1}), which can be excused by the drifters sampling only the top 15 m and the simplified structure of the model. By late May (Figs. 18d and 14c), the gyre covers the whole NGC with the strongest velocities of this transition ($\sim$0.50 m s^{-1} from buoys and $\sim$0.25 m s^{-1} from simulations). The drifter series extended through the full development of the gyre in June and early July (Fig. 14d), and their behavior compares very well with the simulations shown in Fig. 19a.

6. Discussion

The observational part of this work has provided the first directly observed description of the seasonal development of the circulation in the NGC. Hitherto, the only direct observations of the seasonal circulation are the drifter data of Lavín et al. (1997), which sample only the surface layer. More limiting, those data only cover a couple of months in each of the circulation regimes; the full seasonal cycle, with reversal periods, was not analyzed. The asymmetry in duration of the two main regimes, indicated initially by Bray (1988) for a cross section of the NGC, and extended in the horizontal by Carrillo et al. (2001) to describe the gyres, needed to be proved by direct measurements, for their proposal is based on a composite seasonal cycle based on data from several years; more importantly, it is based on geostrophic calculations in a system known to have an important barotropic component. This work has proved by direct observations that this temporal asymmetry exists. The time series of current meters plus the drifters were long enough to establish that the anticyclonic gyre began in mid-October 1995 and ended in mid-April 1996 (6 months), the beginning of the cyclonic period was registered by the drifters in mid-May 1996, and the

ending was observed in late September 1995 by the drifters and the current meters (~4 months). The time span of the autumn transition was observed from late September 1995 to mid-October 1995 (~3 weeks), by the drifters and current meters, while the spring transition was registered by the drifters from mid-April to mid-May (~1 month). This improves the estimate of Carrillo et al. (2001) that the anticyclonic regime lasts from November to March. Although this description of the seasonal cycle of circulation is based on direct observations made in 1995 and 1996, there is evidence that the pattern is repeated every year (Beier 1997; Soto-Mardones 1999; Beier and Ripa 1999; Carrillo et al. 2001).

The hypothesis, put forth in the introduction that the timing and duration of the circulation regimes in the NGC are influenced by the seasonal change of stratification, was investigated numerically by adding vertical mixing to a nonlinearized version of the model of Beier (1997). When entrainment was included in the model, the simulations show better agreement with the observations of sea level and surface temperature. The nonlinear model with entrainment reproduced the observed pattern of circulation, fitting the timing and length of the cyclonic, anticyclonic, and transition regimes; the nonlinear model without entrainment did not reproduce these features. This proves that entrainment caused the cyclonic gyre to exist for a shorter time despite the symmetric forcing. Another case in which entrainment weakens cyclonic circulation is the numerical model, McCreary et al. (1989), of the circulation induced by wind jets blowing offshore normal to the coast, like in the Gulf of Tehuantepec and the Gulf of Papagayo. Their linear model produces dipoles with an anticyclone to the right of the wind, and a cyclone to the left. The latter decays very rapidly in the nonlinear entraining model.

Additional products of the nonlinear entraining model were the mean annual circulation in the NGC, which is predicted to consist of an anticyclonic gyre with speeds ~0.05 m s^{-1} (Fig. 21a), and a net surface flow out of the NGC (Fig. 21a) with a compensating subsurface inflow (not shown). These two features are relevant only when entrainment is used, highlighting the importance of vertical mixing for the thermodynamics and dynamics of the NGC.

The annual-mean baroclinic circulation calculated from hydrographic observations by Bray (1988) and by Carrillo et al. (2001) is cyclonic because, unlike the numerical model, those calculations do not include the barotropic component of the anticyclonic stage of the seasonal cycle. The two-layer exchange is in agreement with the vertical structure of the thermohaline circulation pattern proposed by Bray (1988), with persistent inflowing near-bottom currents over the sills of the archipelago reported by Badan-Dangon et al. (1991) and by M. L. Argote (2000, personal communication).

In the NGC, entrainment maintains a flow of subsurface water to the surface layer, which is drawn from outside the NGC as a mean subsurface influx, which is in turn balanced by a mean surface flow out of the NGC. The interface adjusts with a depression in Delfín Basin and a ridge in the archipelago, producing the mean anticyclonic circulation shown in Fig. 21a. When the mean anticyclonic circulation is added to the sinusoidal circulation produced by the remote forcing of the Pacific Ocean and the seasonal wind, the asymmetry in the duration of the cyclonic and anticyclonic gyres is reproduced.

The temporal mean entrainment of water into the surface layer develops a mean surface current that increases from the head to the mouth and produces, at the mouth of the gulf, a mean horizontal heat flux equal to the mean heat that enters through the surface. In other words, the average circulation pattern is in agreement with the thermodynamic balance in the annual scale, in the sense that the NGC in the annual mean exports heat to the central part of the gulf. The reproduction of the observed heat balance in the average and in the annual scale is a very important achievement of the nonlinear entraining model. However, the full value of $Q_0 = 18$ TW could not be used, most likely because tidal mixing is not included in the model (Beier 1997).

7. Conclusions

Direct measurements show that the seasonal circulation in the northern Gulf of California is dominated by a cyclonic basinwide gyre (~0.35 m s^{-1}) that lasts from June to September (4 months), and an anticyclonic gyre (~0.35 m s^{-1}) lasting from November to April (6 months). The transitions between regimes take about three weeks each.

A two-layer nonlinear numerical model incorporating a seasonal change in stratification gives support to the hypothesis that the asymmetry in the duration of the two main circulation regimes is due to the seasonal variation of stratification of the water column. The predicted duration and timing of the two main regimes, and of the transitional periods, agree very well with the observations. In addition, the model predicts a net anticyclonic circulation, a net subsurface inflow and a compensating surface outflow, and satisfies the observed heat balance. These results indicate the importance of vertical mixing in the dynamics and thermodynamics of the Gulf of California.

Much scope remains for more sophisticated modeling efforts on the dynamics and thermodynamics of the NGC at the annual and at other timescales. Also, alternative explanations for the different durations of the main circulation regimes can be investigated, like a nonsinusoidal forcing at the mouth. In all cases, however, this work indicates that any future numerical models of thermodynamics and circulation must include more realistic parameterizations of vertical mixing.

Acknowledgments. This study was financed by CONACyT (Mexico), through Contracts 3209-T and 26670-T, by FOSIMAC Contract 94/CM-08, and by CICESE. Ship time in the B/O *El Puma* kindly provided by ICMyL, UNAM. We thank Prof. P. Niiler for support with the drifters. Thanks to Mayra Pazos and the Drifter Data Assembly Center at the Atlantic Oceanographic and Meteorological Laboratory of the National Oceanic and Atmospheric Administration, Miami, Florida (NOAA), for providing the drifter data. We thank the enthusiastic crews of the B/Os *Francisco de Ulloa* and *El Puma*. Field work led by Victor Godínez and Salvador Sánchez, with the help of Carlos Flores, Carlos Cabrera, and Joaquín García is appreciated. We appreciate also the comments on a draft of this paper by M. López, G. Marinone, and L. Carrillo. Also, we thank the work of two thorough and helpful referees.

REFERENCES

Argote, M. L., A. Amador, and C. Morales, 1985: Variación estacional de la estratificación en la región norte del Golfo de California. *Memorias de la Reunión Anual 1985,* J. Urrutia-Fucugauchi and J. F. Valdés-Galicia, Eds., Unión Geofísica Mexicana, 334–338.

——, ——, M. F. Lavín, and J. R. Hunter, 1995: Tidal dissipation and stratification in the Gulf of California. *J. Geophys. Res.*, **100,** 16 103–16 118.

Badan-Dangon, A., M. C. Hendershott, and M. F. Lavín, 1991: Underway Doppler current profiles in the Gulf of California. *Eos, Trans. Amer. Geophys. Union,* **72,** 209 and 217–218.

Beier, E., 1997: A numerical investigation of the annual variability in the Gulf of California. *J. Phys. Oceanogr.,* **27,** 615–632.

——, 1999: Estudio de la marea y la circulación estacional en el Golfo de California mediante un modelo de dos capas heterogéneas. Ph. D. thesis, Department of Physical Oceanography, Centro de Investigación Científica y de Educación Superior de Ensenada, Ensenada, México, 64 pp. [Available from Biblioteca de CICESE, Ap. Postal 2732, Ensenada, Baja California, 22800, Mexico.]

——, and P. Ripa, 1999: Seasonal Gyres in the Northern Gulf of California. *J. Phys. Oceanogr.,* **29,** 305–311.

Berón-Vera, F. J., and P. Ripa, 2000: Three-dimensional aspects of the seasonal heat balance in the Gulf of California. *J. Geophys. Res.*, **105,** 11 441–11 457.

Bray, N. A., 1988: Thermohaline circulation in the Gulf of California, *J. Geophys. Res.*, **93,** 4993–5020.

Carrillo, L. E., M. F. Lavín, and E. Palacios-Hernández, 2001: Seasonal evolution of the geostrophic circulation in the Northern Gulf of California. *Estuary Coastal Shelf Sci.*, in press.

Carrillo-Bibriezca, L., 1996: Circulación geostrófica en la región norte del Golfo de California. M.S. thesis, Dept. of Physical Oceanography, Centro de Investigación Científica y de Educación Superior de Ensenada, Ensenada, México, 64 pp. [Available from Biblioteca de CICESE, Ap. Postal 2732, Ensenada, Baja California, 22800, Mexico.]

Castro, R., M. F. Lavín, and P. Ripa, 1994: Seasonal heat balance in the Gulf of California. *J. Geophys. Res.*, **99,** 3249–3261.

García-Córdova, J., C. F. Flores-Cabrera, and J. M. Robles Pacheco, 1996: Datos de CTD obtenidos en la Bahía de Todos Santos, B. C. Campaña BATOS 5. B/O Francisco de Ulloa. Data Rep. CTOFT9603, Comunicaciones Académicas, Serie Oceanografía Física, CICESE, 60 pp.

Godin, G., 1988: *Tides.* Centro de Investigación Científica y de Educación Superior de Ensenada, 290 pp.

Lavín, M. F., and S. Organista, 1988: Surface heat flux in the Northern Gulf of California. *J. Geophys. Res.*, **93,** 14 033–14 038.

——, R. Durazo, E. Palacios, M. L. Argote, and L. Carrillo, 1997: Lagrangian observations of the circulation in the northern Gulf of California. *J. Phys. Oceanogr.*, **27,** 2298–2305.

Lu, P., J. McCreary, and B. Klinger, 1998: Meridional circulation and source waters of the Pacific Equatorial Undercurrent. *J. Phys. Oceanogr.*, **28,** 62–84.

Martínez-Sepúlveda, M., 1994: Descripción de la profundidad de la capa mezclada superficial en el Golfo de California. B.S. thesis, Facultad de Ciencias Marinas, Universidad Autónoma de Baja California, Ensenada, Mexico, 48 pp.

McCreary, J. P., and P. K. Kundu, 1988: A numerical investigation of the Somali Current during the Southwest Monsoon. *J. Mar. Res.*, **46,** 25–58.

——, H. S. Lee, and D. B. Enfield, 1989: The response of the coastal ocean to strong offshore winds: With application to circulation in the Gulfs of Tehuantepec and Papagayo. *J. Mar. Res.*, **47,** 81–109.

——, P. K. Fukamachi, and P. K. Kundu, 1991: A numerical investigation of jets and eddies near eastern ocean boundary. *J. Geophys. Res.*, **96,** 2515–2534.

Organista, S., 1987: Flujos de calor en el Alto Golfo de California. M.S. thesis, Dept. of Physical Oceanography, Centro de Investigación Científica y de Educación Superior de Ensenada, Ensenada, México, 142 pp. [Available from Biblioteca de CICESE, Ap. Postal 2732, Ensenada, Baja California, 22800, Mexico.]

Paden, C. A., C. D. Winant, and M. Abbot, 1991: Tidal and atmospheric forcing of the upper ocean in the Gulf of California, 1. Sea surface temperature variability. *J. Geophys. Res.*, **96,** 18 317–18 359.

Palacios-Hernández, E., M. F. Lavín-Peregrina, S. Sánchez-Mancilla, and V. Godínez-Sandoval, 1997: Campañas oceanográficas y datos de corrientímetros en la región norte del Golfo de California 1994–1996. CICESE Data Rep. CTOFT9701, Comunicaciones Académicas, Serie Oceanografía Física, CICESE, 91 pp.

Ripa, P., 1990: Seasonal circulation in the Gulf of California. *Ann. Geophys.*, **8,** 559–564.

——, 1997: Toward a physical explanation of the seasonal dynamics and thermodynamics of the Gulf of California. *J. Phys. Oceangr,* **27,** 597–614.

Roemmich, D., 1983: Optimal estimation of hydrographic station data and derived fields. *J. Phys. Oceangr.*, **13,** 1544–1549.

Simpson J. H., 1981: The shelf sea fronts: Implications of their existence and behavior. *Philos. Trans. Roy. Soc. London,* **A302,** 531–546.

Soto-Mardones, L., S. G. Marinone, and A. Parés-Sierra, 1999: Time and spatial variability of sea surface temperature in the Gulf of California. *Cienc. Mar.,* **25,** 1–30.